Bromine atom production and chain propagation during springtime Arctic ozone depletion events in Barrow, Alaska

Chelsea R. Thompson,[1,a,b] Paul B. Shepson,[1,2] Jin Liao,[3,a,b] L. Greg Huey,[3] Chris Cantrell[4,c], Frank Flocke[4], and John Orlando[4]

[1]Department of Chemistry, Purdue University, West Lafayette, IN, USA

[2]Department of Earth and Atmospheric Sciences and Purdue Climate Change Research Center, Purdue University, West Lafayette, IN, USA

[3]School of Earth and Atmospheric Sciences, Georgia Institute of Technology, Atlanta, GA, USA

[4]National Center for Atmospheric Research, Boulder, CO, USA

[a]now at: Cooperative Institute for Research in Environmental Sciences, University of Colorado Boulder, Boulder, CO, USA

[b]now at: Chemical Sciences Division, NOAA Earth System Research Laboratory, Boulder, CO, USA

[c]now at: Department of Atmospheric and Ocean Sciences, University of Colorado Boulder, Boulder, CO, USA

Correspondence to: C. R. Thompson (chelsea.thompson@noaa.gov)

Abstract. Ozone depletion events (ODEs) in the Arctic are primarily controlled by a bromine radical-catalyzed destruction mechanism that depends on the efficient production and recycling of Br atoms. Numerous laboratory and modeling studies have suggested the importance of heterogeneous recycling of Br through HOBr reaction with bromide on saline surfaces. However, the gas-phase regeneration of bromine atoms through BrO-BrO radical reactions has been

assumed to be an efficient, if not dominant, pathway for Br reformation and thus ozone destruction. Indeed, it has been estimated that the rate of ozone depletion is approximately equal to twice the rate of the BrO self-reaction. Here, we use a zero-dimensional, photochemical model, largely constrained to observations of stable atmospheric species from the 2009 OASIS campaign in Barrow, Alaska, to investigate gas-phase bromine radical propagation and recycling mechanisms of bromine atoms for a seven-day period during late March. This work is a continuation of that presented in Thompson et al. (2015) and utilizes the same model construct. Here, we use the gas-phase radical chain length as a metric for objectively quantifying the efficiency of gas-phase recycling of bromine atoms. The gas-phase bromine chain length is determined to be quite small, at <1.5, and highly dependent on ambient O_3 concentrations. Furthermore, we find that Br atom production from photolysis of Br_2 and BrCl, which is predominately emitted from snow and/or aerosol surfaces, can account for between 30 – 90% of total Br atom production. This analysis suggests that condensed phase production of bromine is at least as important as, and at times greater than, gas-phase recycling for the occurrence of Arctic ODEs. Therefore, the rate of the BrO self-reaction is not a sufficient estimate for the rate of O_3 depletion.

1 Introduction

The springtime depletion of boundary layer ozone in the Arctic has been the subject of intense research for several decades. Early observations revealed a strong correlation between ozone depletion events (ODEs) and enhancements in filterable bromine (Barrie et al., 1988). This discovery led researchers to propose a mechanism for the bromine-catalyzed destruction of ozone.

$Br_2 + h\nu \rightarrow 2Br$ (R1)

$Br + O_3 \rightarrow BrO + O_2$ (R2)

$BrO + BrO \rightarrow Br_2 \text{ (or } Br + Br) + O_2$ (R3)

This reaction cycle requires an initial source of bromine atoms to the boundary layer. Laboratory and theoretical studies have suggested that Br_2 could be produced through oxidation of bromide present in salt-enriched snow, ice or aerosol surfaces by gas-phase ozone (Hirokawa et al., 1998; Oum et al., 1998b; Gladich et al., 2015).

$O_3 + 2Br^-_{(aq)} + 2H^+_{(aq)} \rightarrow\rightarrow Br_2 + O_2 + H_2O$ (R4)

Field observations by Pratt et al. (2013) using a controlled snow chamber experiment with natural tundra snow collected near Barrow, AK lend further evidence to this mechanism, and also suggest Br_2 production from OH produced photochemically within the snowpack. This mechanism was further explored in the modeling study of Toyota et al. (2014) that suggested an important role for this activation pathway in producing bromine within the snowpack interstitial air.

Once present in the gas-phase, bromine atoms can be regenerated through radical-radical reactions of BrO with XO (where X = Br, Cl, or I), NO, OH, or CH_3OO to propagate the chain reaction and continue the destruction cycle of ozone. If BrO photolyzes or reacts with NO, O_3 is regenerated, and there is a null cycle with respect to O_3. However, although O_3 is not destroyed, these two pathways represent efficient routes for Br atom propagation. Thus R3 serves to make R2 effective in destruction of O_3. At the same time, Br atoms could be recycled through heterogeneous reactions of HOBr with bromide in the condensed phase to release Br_2 to the gas-phase via the now well-known "bromine explosion" mechanism (Vogt et al., 1996; Tang and McConnell, 1996; Fan and Jacob, 1992).

$$BrO + HO_2 \rightarrow HOBr + O_2 \quad \text{(R5)}$$

$$HOBr_{(g)} \rightarrow HOBr_{(aq)} \quad \text{(R6)}$$

$$HOBr_{(aq)} + Br^-_{(aq)} + H^+_{(aq)} \leftrightarrow Br_{2(aq)} + H_2O \quad \text{(R7)}$$

$$Br_{2(aq)} \rightarrow Br_{2(g)} \quad \text{(R8)}$$

Evidence for reaction sequence R5 – R8 has been provided through laboratory studies, which found that Br_2 was produced when frozen bromide solutions were exposed to gas-phase HOBr (Huff and Abbatt, 2002; Adams et al., 2002). This mechanism is believed to proceed rapidly to produce Br_2 so long as sufficient bromide is present in an accessible condensed phase. The efficiency of this heterogeneous recycling mechanism has also been found to have a dependence on the acidity of the surface, as was shown using natural environmental snow samples in Pratt et al. (2013) and investigated in the modeling studies of Toyota et al. (2011, 2014), in a manner that is consistent with the stoichiometry of Reaction R7.

To efficiently sustain the ozone destruction cycle to the point of near complete loss of boundary layer ozone ($[O_3] < 2$ ppb), bromine atoms must be continually recycled through some combination of the above mechanisms. The gas-phase reaction cycle described by Reactions R1 – R3 has generally been considered to be the dominant pathway for Br reformation following the initial activation of Br_2 from the surface (the mechanism for which is still not fully understood). Thus, it has been assumed that the rate of ozone destruction can be estimated as Equation 1 (see Equation 15 in Hausmann and Platt, 1994, Equation 3 in Le Bras and Platt, 1995, and Equation 7 in Zeng et al., 2006), or as Equation 2 if chlorine chemistry is considered through Reaction R9 (Equation IX in Platt and Janssen, 1995).

$$-\frac{d[O_3]}{dt} = 2 \cdot k_3 \cdot [BrO]^2 \quad (1)$$

$$-\frac{d[O_3]}{dt} = 2(k_3 \cdot [BrO]^2 + k_9 \cdot [BrO] \cdot [ClO]) \quad (2)$$

102 $BrO + ClO \rightarrow Br + OClO$ (R9)

103 However, these approximations assume that the ozone destruction rate is dominated by the BrO
104 + XO reaction, which in turn necessitates efficient gas-phase recycling of Br; therefore, a
105 relatively long bromine chain length would be required to account for observed rates of ozone
106 destruction. It is, however, possible that Br atoms are generated mostly by Br_2 photolysis,
107 followed by BrO termination, e.g. by R5, in which case a short gas-phase bromine radical chain
108 length would be implied. The chain length for any process depends on the rates of the
109 propagation relative to the production and destruction reactions (Kuo, 1986). It is important to
110 note that the chain length refers to radical propagation reactions occurring solely in the gas phase,
111 and is a quantity completely independent of any condensed phase chemistry. In the stratosphere,
112 the Br/BrO catalytic cycle can have a chain length ranging from 10^2 to 10^4 (Lary, 1996). In the
113 troposphere, there is significantly less solar radiation and many more available sinks; thus,
114 radical chain lengths can be much shorter. For example, the chain length of the tropospheric
115 HO_x cycle has been estimated to be ~ 4 – 5 (Ehhalt, 1999; Monks, 2005), increasing to 10 – 20
116 near the tropopause (Wennberg et al., 1998). The halogen radical chain lengths in the Arctic
117 troposphere have so far not been determined, thus, it is difficult to evaluate whether Equations I
118 and II are appropriate for estimating ozone depletion rates.

119 The importance of heterogeneous reactions for recycling reactive bromine has been
120 demonstrated in the recent literature (see review by Abbatt et al., 2012). Modeling studies using
121 typical Arctic springtime conditions to simulate ODEs have concluded that ozone depletion
122 cannot be sustained without considering the heterogeneous recycling of reactive bromine on
123 snow or aerosol surfaces (e.g., Michalowski et al., 2000; Piot and Von Glasow, 2008; Liao et al.,
124 2012; Toyota et al., 2014). Michalowski et al. (2000) determined that the rate of ozone depletion

in their model was limited by the mass transfer rate of HOBr to the snowpack (effectively, the rate at which Br is recycled through the heterogeneous mechanism) and that the depletion of ozone is nearly completely shut down when snowpack interactions are removed. Piot and von Glasow (2008) simulated ozone depletion using the one-dimensional MISTRA model and concluded that major ODEs (defined as complete destruction within 4 days) could only be produced if recycling of deposited bromine on snow is included. Without heterogeneous recycling on the snowpack, the BrO_x termination steps and irreversible loss of HOBr and HBr to the surface prohibits the occurrence of an ODE. More recently, using HOBr observations from Barrow during OASIS, Liao et al. (2012b) found that a simple photochemical model over-predicted observed HOBr during higher wind events (> 6 m s^{-1}), ostensibly due to an under-predicted heterogeneous loss to aerosol in the model, and concluded that their field observations support the hypothesis of efficient recycling back to reactive bromine via this mechanism.

While it is evident that the reactions occurring on snow and aerosol surfaces are likely the initial source of halogen species to the polar boundary layer and that heterogeneous bromine recycling on these surfaces must be considered for HOBr and HBr (as well as $BrNO_2$ and $BrONO_2$ in higher NO_x environments), the relative importance of gas-phase recycling of bromine atoms is uncertain, as demonstrated by the use of gas-phase radical reaction rates to estimate the ozone depletion rate. The goal of this work was to investigate gas-phase Br atom propagation in terms of the bromine chain length in comparison to the production of Br atoms through photolysis of Br_2 and BrCl, which are predominantly produced directly from surface emissions. Here, we present results from our study using a zero-dimensional model constrained with time-varying measurements of molecular halogens, HOBr, O_3, CO, NO, NO_2, and VOCs from the 2009 Ocean-Atmosphere-Sea Ice-Snowpack (OASIS) campaign in Barrow, Alaska.

This work builds on the analysis presented in Thompson et al. (2015) using the same model framework. By constraining our model with observations, we were able to conduct an in-depth study of the halogen atom recycling occurring under varying conditions that were observed during the campaign.

2 Experimental

2.1 Measurements and Site Description

The analysis presented herein utilizes observations conducted during the OASIS field campaign that occurred during the months of February through April of 2009 in Barrow, AK. The goal of the OASIS study was to investigate the chemical and physical processes occurring within the surface boundary layer during ozone and mercury depletion events in polar spring. This study resulted in the largest suite of simultaneous and co-located atmospheric measurements conducted in the Arctic near-surface atmosphere to date, and represents a unique opportunity for in-depth examination of a multitude of chemical interactions in this environment.

Atmospheric measurements were conducted from instrument trailers located near the Barrow Arctic Research Consortium (BARC) facility on the Naval Arctic Research Laboratory (NARL) campus. Winds arriving at the site are primarily northeasterly, from over the sea ice, and thus represent background conditions with influence from natural processes and snow-air interactions. Winds occasionally shift to westerly, bringing local emissions from the town of Barrow to the site, however these isolated events are easily identifiable by coincident enhancements in both NO_x and CO.

Measurements of molecular halogens, HOBr, NO, NO_2, O_3, CO, and VOCs were used to constrain the model employed in this analysis. Instrumental methods for these measurements

171 have all been described elsewhere, thus, only a brief description is provided here. Inorganic
172 halogen species (Br_2, Cl_2, BrO, and HOBr) were measured by chemical ionization mass
173 spectrometry with I^- ion chemistry as described in Liao et al. (2011, 2012, 2014); O_3, NO, and
174 NO_2 were measured by chemiluminscence (Ridley et al., 1992; Ryerson et al., 2000). CO was
175 measured using a standard commercial CO analyzer (Thermo Scientific) with infrared absorption
176 detection, and formaldehyde (HCHO) was measured at 1 Hz frequency using a tunable diode
177 laser absorption spectrometer, as described in Fried et al. (1997) and Lancaster et al. (2000). A
178 large suite of organic compounds was measured in situ by fast GC-MS (Apel et al. 2010) and via
179 whole air canister samples with offline GC-MS (Russo et al., 2010).
180
181 **2.2 Model Description**
182 The model used for this study is a zero-dimensional box model developed using the
183 commercial software FACSIMILE. A detailed description of the model can be found in
184 Thompson et al. (2015). We will describe the model only briefly here.
185 Our model consists of 220 gas-phase reactions and 42 photolysis reactions, representing
186 much of the known gas-phase chemistry occurring in the Arctic, including the important halogen,
187 HO_x, NO_x and VOC chemistry associated with ozone depletions. The model also includes an
188 inorganic iodine reaction scheme adapted from McFiggans et al. (2000, 2002), Calvert and
189 Lindberg (2004) and Saiz-Lopez et al. (2008). Although IO has not been unambiguously
190 measured in the High Arctic above the ~1.5 – 2 pptv detection limit of LP-DOAS (long-path
191 differential optical absorption spectroscopy), observed enhancements in filterable iodide and
192 total iodine suggest that iodine chemistry is active to some extent in this region (Sturges and
193 Barrie, 1988; Martinez et al., 1999; Mahajan et al., 2010; Hönninger, 2002). Recently, I_2 has

been detected at tens of pptv within the snowpack interstitial air near Barrow, AK and at ≤0.5 pptv in the near surface air by I^- CIMS, providing direct evidence supporting the presence of at least low levels of iodine chemistry (Raso et al., 2016). In our previous study (Thompson et al., 2015), we investigated the impact of two different hypothetical levels of iodine. Here, we investigate only the "Low Iodine" scenario for certain calculations, in which a diurnally varying I_2 flux is incorporated such that average daytime mole ratios of IO remain near 1 pptv for the majority of the simulation. These levels of IO are realistic given our current knowledge based on the work of Hönninger (2002) and Raso et al. (2016).

All gas-phase rate constants used in this model were calculated for a temperature of 248 K, consistent with average daytime conditions in Barrow for the period simulated. Although some gas-phase reactions can exhibit a significant temperature dependence, we chose not to incorporate variable temperatures into our model. This is justified in this case because ambient temperature in Barrow for the week of 25 March 2009 varied by less than 10 K between the maximum and minimum recorded daily temperatures. The radical oxidation and radical-radical reactions that are of primary importance here do not have a large temperature dependence (Atkinson et al., 2006, 2007); for example, a variability of 10 K imposes an ~1% change on the rate of ethane oxidation by Cl atoms and a <4% change on the rate of the BrO + BrO radical self-reaction. Most radical-radical reactions have only a small negative-temperature dependence. Furthermore, and as mentioned previously, the major non-radical chemical species driving the model are highly constrained to observations and are not allowed to freely evolve. Table 1 contains an abbreviated list of the reactions included in the model, showing only those reactions that are central to the production, propagation, and termination of bromine radical chemistry that is the focus of this study. A complete list of reactions can be found in Thompson et al. (2015).

The model is configured to simulate 7 days during late March, 25 through 31 March, that include a period of depleting ozone, a full ozone depletion ($[O_3] < 2$ ppbv) lasting ~ 3 days, and recovery. The O_3 time-series for this period is shown in Figure 1A, along with radiation as a reference (all plots are in Alaska Standard Time). We constrain the model to observations for this time period by reading in time-varying data sets of O_3, C_2H_2, C_2H_4, C_2H_6, C_3H_8, C_3H_6, *n*-C_4H_{10}, *i*-C_4H_{10}, HCHO, CH_3CHO, CH_3COCH_3, methyl ethyl ketone (MEK), Cl_2, Br_2, HOBr, NO, NO_2, and CO at ten-minute time steps. All other gas-phase species are allowed to freely evolve. Surface fluxes (represented as volumetric fluxes) are used for HONO and I_2 and are scaled to $J(NO_2)$ as a proxy for radiation as both of these species are likely to be produced photochemically. Further discussion regarding HONO can be found in Thompson et al. (2015).

Photolysis rate constants (*J* coefficients) for many of the species included were calculated during OASIS using the Tropospheric Ultraviolent and Visible Radiation model from measurements of down-welling actinic flux conducted throughout the campaign (Shetter and Müller, 1999; Stephens et al., 2012). Estimates of J_{max} in the Arctic for OClO were taken from Pöhler et al. (2010), for HOCl from Lehrer et al. (2004), and for $CHBr_3$ from Papanastasiou et al. (2014). J_{max} values for the iodine compounds were calculated according the work of Calvert and Lindberg (2004), which also simulated conditions for late March in Barrow, Alaska. Time-varying *J* coefficients for O_3 and NO_2 were read into the model at 10-minute time steps. All other photolysis reactions were scaled to $J(NO_2)$ in the modeling code using the maximum *J* coefficients (J_{max}) for 25 March (a clear-sky day) as a scaling factor. For cloudy days, this method assumes that *J* coefficients for other photolytically-active species are attenuated in a manner that is proportional to $J(NO_2)$.

In the initial development of the model, heterogeneous reactions of halogen species occurring on aerosol and snowpack surfaces were included, as well as mass transfer and dry deposition for certain species using the method and mechanism of Michalowksi et al. (2000). This mechanism assumes aqueous phase kinetics for those reactions occurring within a uniformly distributed quasi-liquid layer (QLL), in a similar fashion as numerous other models (e.g., Piot and von Glasow, 2008; Thomas et al, 2011; Toyota et al., 2014). It was originally intended to utilize this multiphase chemistry to produce halogen radical precursors. However, the heterogeneous production mechanisms could not reproduce observed Br_2 or Cl_2 from OASIS. This reflects the complex but not fully understood condensed phase chemistry and physics that leads to production of Br_2 (and Cl_2) (Abbatt et al., 2012; Domine et al., 2013; Pratt et al., 2013). Additionally, the current knowledge of the physical properties of the QLL and the location of liquid-like surfaces on snow grains would seem to invalidate the aforementioned assumptions on which many of the current heterogeneous models are based (Domine et al., 2013), specifically that the chemistry occurs in a liqui-like environment on snow grains. Indeed, Cao et al. (2014), adopted a simplified heterogeneous chemistry mechanism in their modeling of Arctic ozone depletion, wherein they use the mass transfer of HOBr to the surface as the rate-limiting step in Br_2 production, citing the lack of suitable reaction mechanisms with which to properly simulate condensed phase chemistry on snow/ice. Admittedly, our model is also not able to capture these complex heterogeneous processes. However, as discussed thoroughly by Domine et al. (2013), even our most complex state-of-the-art snow chemistry models are neither physically nor chemically accurate, and rely upon a variety of adjustable parameters to produce reasonable results, because of the lack of fundamental understanding of the actual phase and physical and

chemical environment in which the chemistry is occurring. It is thus clear to state that the kinetics of the individual reactions in such a case cannot be reliably simulated.

In light of the limitations of all models of cryosphere photochemistry, a strength of this study, and opportunity, rests with the fact that we have observations of key halogen species, including Br_2, Cl_2, BrO, ClO, HOBr, as well as VOCs, NO_x, OH and HO_2. Therefore, to study the gas phase recycling discussed in the Introduction, in this work Br_2 and Cl_2 concentrations were fixed at the observed levels (see Thompson et al., 2015 for further discussion) and were not produced via heterogeneous chemistry. During a period spanning a portion of 29 and 30 March, Br_2 observations are not available due to instrument instability. Here, we have filled in the missing portion of data with average daytime Br_2 values based on observations from 27 and 28 March and the morning data available for 29 March, and use average nighttime values for the night of 29/30 March using the observations from the two adjacent nighttime periods. The filled-in values for Br_2 result in reasonable agreement between modeled and observed BrO for this period. In the analyses presented in Figures 3 and 5 – 10 we have indicated this period of missing and filled-in Br_2 values with a shaded box. Due to the sparseness of BrCl observations during OASIS, only daytime BrCl was used as produced in the model multiphase mechanism. While we do not argue that the production mechanism for BrCl is accurate, the daytime simulated BrCl mole ratios of 0 – 10 pptv are in approximate agreement with the available data for the campaign. In any case, according to our model, BrCl was not a significant source of either Br or Cl atoms relative to Br_2 and Cl_2.

Though we do not use the heterogeneous chemistry module for any chemical production (other than BrCl), deposition and mass transfer is a significant and critical sink for certain species. Thus, we do make use of this aspect of the multiphase portion of the model, as described

below. The dry deposition velocity of O_3 to the snowpack is estimated at 0.05 $cm \cdot s^{-1}$, consistent with previous measurements and modeling studies (Gong et al., 1997; Michalowski et al., 2000; Helmig et al., 2007; Cavender et al., 2008), though it is recognized that there is large uncertainty with this parameter from field observations (Helmig et al., 2007, 2012). Assuming a boundary layer height of 300 m, this corresponds to a transfer coefficient, k_t, of 1.67×10^{-6} s^{-1}. Dry deposition velocities for the stable Arctic environment have not been determined for the halogen acids (HBr, HCl, HOBr, HOCl, HOI), therefore we use the estimation method of Michalowski et al. (2000) and assume a deposition velocity that is 10 times greater than for O_3, leading to a k_t of 1.67×10^{-5} s^{-1}. We assume an equivalent k_t for the oxidized nitrogen compounds (HNO_3, HO_2NO_2, HONO, N_2O_5, $BrNO_2$, and $BrONO_2$). The mass transfer coefficient of atmospheric species to the particle phase is calculated as a first-order process as described in Jacob (2000). The concentration of aerosol surface area used was 3.95×10^{-7} cm^2 cm^{-3} as calculated by Michalowski et al. (2000) from measurements made at Alert by Staebler et al. (1994), with a maximum aerosol radius of r = 0.1 μm. These levels are also consistent with observations of aerosol surface area at Barrow, which ranged between 9×10^{-8} cm^2 cm^{-3} and 40×10^{-7} cm^2 cm^{-3} (Liao et al. 2012b). We recognize, however, that this constant level of aerosols imparts a constant loss rate in the model and does not take into account any variability in the deposition strength. Because many of these species are lacking empirically-derived deposition velocities (e.g, HOBr), there is necessarily large uncertainty in these values, and it is not possible at this time to ascertain whether the uncertainty associated with the deposition velocity estimation is greater or less than the uncertainty imposed by using a constant aerosol surface area. Liao et al. (2012b) did use time-varying aerosol surface area from observations at Barrow, however, they suggested that simple parameterization of deposition of HOBr to aerosols was insufficient for

accurately simulating HOBr (further discussion of HOBr is in Section 3.1). Given the highly simplified nature of the surface deposition in our model, we do not attempt to differentiate between deposition to aerosols and snow, and instead we lump these two terms together under the "surface deposition" umbrella. However, while we mostly constrain the model to observed HOBr, the comparison to simulated HOBr using these values is instructive.

3 Results and Discussion

3.1 Comparison of modeled and observed Br_2, BrO, HOBr, and HO_2

This work focuses on the propagation and production mechanisms of Br atoms, and thus it is critical that our model accurately simulates BrO and Br_2 at mixing ratios that are consistent with observations. Figures 1B and 1C show comparisons between simulated mixing ratios (black trace) of Br_2 and BrO compared to the measured values during this time (red data) by chemical ionization mass spectrometry (CIMS) (Liao et al., 2012b). Modeled BrO is presented as hourly averages. In the model, Br_2 is fixed to time-varying observations, whereas BrO is produced strictly through the gas-phase photochemical reactions. The model captures the overall temporal profile and magnitude of BrO throughout the period. It should be noted, however, that the uncertainty in the BrO measurements is large during ODEs as the observed values are very near the detection limit (LOD of ~2 pptv with uncertainty of -3/+1 pptv near the LOD).

Br_2 mixing ratios reach 2 – 12 pptv (Figure 1B) during the daytime. Given the short lifetime of Br_2 resulting from rapid photolysis, these daytime mixing ratios imply a large surface flux, that in turn produces the BrO mole ratios observed. These Br_2 levels are consistent with previous Arctic measurements that observed daytime Br_2 up to 27 pptv (Foster et al., 2001) and agree well with the "uncorrected" Br_2 data reported in Liao et al. (2012a, 2012b) for this period.

It has been suggested that daytime Br_2 greater than the CIMS instrumental detection limit (~1 pptv) is an artifact of HOBr conversion to Br_2 on the instrument inlet using an aircraft inlet (Neuman et al., 2010), however, for the instrument configuration employed during OASIS, it is not clear how much, if any, of the Br_2 signal is a result of HOBr reactions on instrument surfaces.

An estimate of the effective mixing height of Br_2 can be calculated using the method of Guimbaud et al. (2002) and using an average measured diffusivity during OASIS of 1500 $cm^2\ s^{-1}$ (R. Staebler, personal communication, 2015). By assuming that photolysis is the dominant loss mechanism controlling the Br_2 mid-day lifetime in a stable boundary layer typical of Arctic conditions, the daytime effective mixing height is ~1.85 m. This also assumes that the snowpack is the primary source of Br_2 emissions, which is consistent with previous assumptions for the aldehydes (Sumner et al., 1999; Guimbaud et al., 2002) and is supported by direct empirical evidence of the tundra snowpack being a relatively strong source of Br_2 (Pratt et al., 2013). Enhanced Br_2 within the snowpack interstitial air has also been predicted from the modeling studies of Toyota et al. (2011, 2014). From this estimation, the majority of the Br_2 present at the surface would remain at the height of the instrument inlet (~1 m) in the sunlit periods. If aerosols do represent a significant source of Br_2 as has been hypothesized, and inferred indirectly from bromide depletion in sea salt aerosols (Sander et al., 2003), then one would expect enhanced Br_2 to be present throughout the height of the boundary layer. In our highly constrained model, daytime Br_2 mixing ratios greater than 1 pptv are necessary to reproduce observed BrO, therefore, this modeling study suggests that Br_2 should indeed be present and above the instrument detection limit during the daytime. Br atoms are predicted at concentrations ranging from 1×10^7 to 3×10^9 molecules cm^{-3}. The hourly averaged model output for Br is shown in Figure 2D. No direct measurements of Br atoms are available with which to compare, though

these values are within the range of estimates determined by Jobson et al. (1994) and Ariya et al. (1998).

In the case of HOBr, our model originally simulated this species based on the known gas-phase sources and sinks (including photolysis) and deposition/uptake to surfaces as described above. As shown in Thompson et al. (2015), and again in Figure 2A, given the observed Br_2 mixing ratios, the model greatly overestimated HOBr. Liao et al. (2012b) also simulated inorganic bromine species from the OASIS campaign using a simple steady-state model and experienced that their model also overestimated the observed HOBr, with the overestimation becoming especially pronounced during periods of higher winds. They suggested a faster heterogeneous loss to aerosols or blowing snow that was not represented in their model, despite utilizing time-varying aerosol surface area from observations. For the majority of the results presented in this work, we chose to operate our model constrained to HOBr observations, as illustrated in Figure 2B. Figure 2C shows modeled HOBr obtained by adjusting the deposition to aerosols based on daily wind speeds, and tuned to provide reasonable agreement with observations. This resulted in smaller deposition rates on 25 through 27 March when winds were calm, and higher deposition rates on 29 through 31 March when winds were up to 9 m/s. This method allowed us to calculate the importance of surface deposition of HOBr relative to photolysis as a sink for this compound, but the constrained version of the model was used for all other calculations, e.g. for the chain length calculations.

HO_2 is essential for the heterogeneous recycling of bromine (via Reactions R5 – R7). Therefore, it is important that our model provides a reasonable estimation of HO_2 for this analysis. In Figure 1E we show a comparison of simulated, hourly-averaged HO_2 (black trace) and observed HO_2 from OASIS for this period (red data), measured using a CIMS developed for

376 peroxy radicals (Edwards et al., 2003). Our model captures the diurnal cycle of HO_2 and the
377 daily fluctuations observed. Simulated HO_2 is on the lower limit of observations for 25 and 29
378 March, and does not reach the maximum mixing ratios observed. The model also somewhat
379 overpredicts HO_2 on 28 through 30 March, however, the model values are within the stated 25%
380 - 100% range of uncertainty of the measurement.
381
382 **3.2 Chain length**
383 The ozone destruction cycle as described in Reactions R1 – R3 is a chain reaction
384 mechanism catalyzed by BrO_x. The effectiveness of a catalytic cycle can be can be quantified by
385 considering the chain length, that is, the number of free radical propagation cycles per
386 termination or per initiation. The radical chain length is a metric that refers solely to gas phase
387 reactions (Monks, 2005). We have not, until the OASIS2009 campaign, had the high quality
388 measurements available to enable a reliable estimation of the bromine radical chain length in the
389 Arctic.
390 The length of the chain in a radical propagation cycle is limited by termination steps that
391 destroy the chain carriers and result in relatively stable atmospheric species. Thus, the chain
392 length can be defined as the rate of propagation divided by the rate of termination. Alternatively,
393 the chain length can also be calculated using the rate of initiation. If the total bromine radical
394 population is at steady-state, the rate of initiation is equal to the rate of termination; thus, for
395 short-lived radical species, the two methods for calculating chain length should be approximately
396 equal.
397 Method 1: $$\Phi = \frac{\Sigma(\text{Rates of propagation})}{\Sigma(\text{Rates of termination})} \quad (3)$$
398 Method 2: $$\Phi = \frac{\Sigma(\text{Rates of propagation})}{\Sigma(\text{Rates of initiation})} \quad (4)$$

We used our model to calculate the chain length for bromine radical propagation across the 7-days of the simulated period using both Method 1 and 2 as shown in Equations 5 and 6. Because bromine radicals are generated photolytically, the chain length is calculated for daytime only, defined here as approximately 7:00 to 20:00 Alaska Standard Time (AKST).

Method 1:

$$\Phi_{Br} = \frac{\begin{array}{l}(2k[BrO]^2 + J_{BrO}[BrO] + k[BrO][ClO] + \\ k[BrO][IO] + k[BrO][CH_3OO] + \\ k[BrO][OH] + k[BrO][O(^3P)] \\ + k[BrO][CH_3COOO] + k[BrO][NO])\end{array}}{\begin{array}{l}(k[Br][HO_2] + k[Br][C_2H_2] + k[Br][C_2H_4] \\ + k[Br][C_3H_6] + k[Br][HCHO] + k[Br][NO_2] \\ + k[Br][CH_3CHO] + k[Br][C_3H_6O] + k[Br][C_4H_8O] \\ + k[Br][CH_3OOH] + k[BrO][HO_2] + k[BrO][CH_3OO] \\ + k[BrO][C_3H_6O] + k[BrO][NO_2])\end{array}} \quad (5)$$

Method 2:

$$\Phi_{Br} = \frac{\begin{array}{l}(2k[BrO]^2 + J_{BrO}[BrO] + k[BrO][ClO] + \\ k[BrO][IO] + k[BrO][CH_3OO] + \\ k[BrO][OH] + k[BrO][O(^3P)] \\ + k[BrO][CH_3COOO] + k[BrO][NO])\end{array}}{\begin{array}{l}(2J_{Br2}[Br_2] + J_{BrCl}[BrCl] + J_{HOBr}[HOBr] + J_{BrONO2}[BrONO_2] \\ + J_{IBr}[IBr] + J_{BrNO2}[BrNO_2] + J_{CHBR3}[CHBr_3] + \\ k[HBr][OH] + k[CH_3Br][OH] + k[CHBr_3][OH])\end{array}} \quad (6)$$

Termination reactions for bromine include those reactions that are sinks for either Br and BrO, since Br and BrO rapidly interconvert. Here, photolysis of BrO and the BrO + NO reaction is included in the numerator because they are efficient at reforming Br and propagating the chain; however, these reactions do not result in a net loss of ozone. Photolysis of BrO produces atomic oxygen that reacts with O_2 to form O_3, and NO_2 can photolyze to similarly reform O_3. Therefore, it should be noted that if we omit these reactions and consider only those that result in a net O_3 loss, it would be expected that the chain length would be shorter. Indeed, model simulations were

performed without these two terms and the determined chain lengths were on average 80% lower than those presented here. BrO reaction with CH_3OO is included in both the numerator and denominator in Equation 5 because this reaction has two channels, one that propagates the Br chain and one that terminates it.

In Figure 3, we present the hourly-averaged results of these calculations for the Base Model, which show that the two methods for calculating bromine chain length are in reasonably good agreement, although there are small differences between the two methods throughout the time-series. This agreement is a test of our basic understanding of the radical chemistry. The inset graph in Figure 3 shows a linear regression of the two methods for the chain length calculation. The coefficient of determination (r^2) of 0.93 confirms the good temporal agreement between the two methods. However, the slope of 0.68 indicates that Method 1 is generally higher than Method 2 throughout (with some periods of exception). This offset reveals that either Method 1 is slightly overestimating the chain length, or that Method 2 is underestimating it. The numerator is identical in Equations 5 and 6, therefore, the denominator must be driving this discrepancy, with either the denominator term in Method 1 too low or the denominator term in Method 2 too high (or some combination thereof). If it's the case that the Method 1 denominator is too low, then it must be concluded that there are important BrO_x terminations that are missing from the calculation. If, however, the denominator of Method 2 is too high, this would imply that our measurements of these BrO_x precursors are too high, which, as discussed above, is a known possibility at least for the Br_2 measurements. The photolysis of Br_2 is the dominant initiation pathway (see Section 3.3), therefore, the Method 2 chain length calculation would be the most sensitive to Br_2 measurement inaccuracies.

In Equation 6, we included photolysis of the most prevalent organobromine compound bromoform for completeness, though it has been recognized for many years that the rate of Br atom production from this pathway is small (e.g., ~ 100 molecules·cm^{-3}·s^{-1} for bromoform at mid-day) compared to Br atom production from Br_2 photolysis (~1.3x10^7 molecules·cm^{-3}·s^{-1} at mid-day assuming 5 pptv of Br_2). Photolysis of bromine nitrate ($BrONO_2$) and nitryl bromide ($BrNO_2$) are also included, however, the prevalence of and production of these compounds in the Arctic is highly uncertain, and no observations of these species in the Arctic have been published to date with which to compare to our modeled mixing ratios. Inclusion of these terms at the modeled $BrONO_2$ and $BrNO_2$ mixing ratios has a small effect on the calculated chain length that cannot account for the discrepancy between the two methods.

The median bromine chain-length in the Base simulation, averaging the results from Method 1 and Method 2, is ~1.2 across daylight hours (7:00 to 21:00 AKST) and ~2 for mid-day, defined for this purpose as approximately 12:00 until 18:00 AKST, when $[O_3] \geq 5$ ppbv. In comparison, the bromine chain length is ~0.4 when $[O_3] < 5$ ppbv (Figure 3). In other words, the chain cannot be maintained when $[O_3] < 5$ ppbv. Under these conditions, Br atoms readily terminate, e.g. via reaction with CH_3CHO (see below). 29 March exhibits an early morning enhancement in the chain length. This morning spike appears to correlate with a similar sharp increase in ozone. Br_2 accumulates during the nighttime hours, resulting in the highest Br_2 concentrations in the early morning hours (Figure 1B). When the sun rises, Br_2 photolyzes rapidly, releasing a pulse of reactive bromine that converts to BrO in the presence of ozone. This, in concert with the coincident increase in ozone, can explain the enhanced chain length during the early morning hours.

476 Overall, midday bromine chain lengths remain near or below 2 during background O_3
477 days. This implies that, for these days, ozone depletion is strongly dependent upon initiation
478 processes, and most BrO radicals produced terminate the chain via reactions R5 and R10 (below)
479 in less than two cycles. Reaction R12 (below) will also efficiently terminate the chain, however,
480 the relative importance of R10 and R12 depend upon the relative abundances of BrO and Br. For
481 background O_3 days, such as 29 and 30 March, [BrO] > [Br], thus, R10 > R12. The low chain
482 lengths calculated here are surprising, given that it has been generally accepted that Br is
483 recycled efficiently in the gas-phase. That it appears this is not the case supports the conclusions
484 of Michalowski et al. (2000), Piot and von Glasow (2008), and Toyota et al. (2014) that
485 heterogeneous recycling through the "bromine explosion", which emits Br_2 and BrCl from
486 surface reactions, is of critical importance to sustain ODEs occurring at the surface.
487 A question to address regarding the relatively small chain length calculated for Br is to
488 what extent the chain length is dependent on NO_2. As discussed in Thompson et al. (2015) and
489 further investigated in Custard et al. (2015), NO_2 at Barrow can be greater and more variable
490 than at very remote sites due to its proximity to anthropogenic emissions sources. We find that
491 the chain length calculation is relatively insensitive to NO_2 concentrations and so it is robust for
492 the range of conditions encountered at Barrow. This is shown in detail in Custard et al. (2015).
493 As discussed by Custard and coworkers, while NO_2 can inhibit the bromine chain through
494 reactions R10 and R12 (i.e., decreasing the chain length), enhanced NO_2 will also reduce
495 available HO_2, thereby decreasing the HO_2 available to terminate the chain (i.e., increasing the
496 chain length). While the Method 2 calculation does not contain NO_2 in the denominator, the
497 absolute [BrO] is NO_x-dependent because of reaction R10 (Custard et al., 2015), and it is through
498 this effect that high NO_x mixing ratios act to decrease the rate of O_3 depletion. In the natural

environment, Br_2 production can potentially also be NO_x-dependent, e.g. via reaction R11, followed by R7. While our model does not *simulate* the condensed phase processes, it is sensitive to them, since the model is constrained to the product of those processes, Br_2.

$$BrO + NO_2 \rightarrow BrONO_2 \quad \text{(R10)}$$

$$BrONO_{2(aq)} + H_2O \rightarrow HOBr + HNO_3 \quad \text{(R11)}$$

$$Br + NO_2 \rightarrow BrNO_2 \quad \text{(R12)}$$

However, for the period of 26 through 30 March, NO_x was relatively low, and the relatively good agreement between the two calculation methods further supports our conclusion.

To investigate how chemical interactions with chlorine and iodine affect the bromine chain length, a series of simulations was performed by varying the combinations of halogens present in the model. The bromine chain length was determined for scenarios with only Br, Br and Cl (Base Model), Br and Iodine, and Base with Iodine. Simulations without chlorine were performed simply by removing Cl_2, while simulations with iodine were performed by incorporating the I_2 flux as described in Section 2.2. No other adjustments were made to the model for these sensitivity runs.

Table 2 shows the results for both chain length calculation methods (i.e., Equations 5 and 6) for the different halogen combinations for the three days when ozone was present near background values: 25, 29 and 30 March. For the Base scenario ("Br and Cl"), the average of the median daily values for the bromine chain length is 1.43 and 1.05 for Method 1 and Method 2, respectively. In comparison with the "Br Only" run, Cl chemistry does not induce a net increase in the Br chain length, but rather causes a slight decrease. Cl chemistry can increase Br radical propagation through the addition of the BrO + ClO cross-reaction and enhancement of the BrO + CH_3OO radical propagation terms. However, Cl chemistry can also increase the concentration of

522 reactive bromine sinks, such as aldehydes (e.g., propanal and butanal, which were free to evolve
523 in our model; HCHO and CH_3CHO are fixed to observations) and HO_2 (see Thompson et al.,
524 2015). Iodine has the effect of increasing the Br chain length. When low levels of iodine are
525 added to the "Br Only" simulation, the chain increases from 1.52 to 1.59 in the Method 1
526 calculation, primarily due to the very fast cross-reaction between IO and BrO. The addition of
527 Cl to the "Br and I" simulation imparts a slight decrease to the Br chain length. This may be
528 explained by the competition between BrO and ClO for reaction with NO and/or IO, as well as
529 the additional Br sinks in the presence of Cl chemistry. Regardless, overall there is more Br
530 available for reaction with O_3 when Cl is present due to the interhalogen reactions, thereby
531 increasing the rate of ozone depletion (see Thompson et al., 2015 for further discussion on ozone
532 depletion rates).

533 There are several conclusions that can be drawn from Figure 3 and Table 2: 1) there is a
534 distinct difference in bromine chain length between O_3-depleted and non-depleted days with a
535 significantly larger chain length when ozone is present, and 2) for all simulations, the average
536 bromine chain is much shorter than expected (given that gas-phase recycling has, to date, been
537 assumed to be highly efficient). The chain length is greatest when ozone is present because
538 many of the species that propagate the Br chain (e.g., BrO, ClO, IO, and to a lesser extent OH
539 and CH_3OO) require O_3 for production. Although the relationship between bromine chain length
540 and BrO is not straightforward due to the multitude of interactions between BrO and other
541 species that either propagate or terminate the chain, the chain length does exhibit a rough
542 dependence on [BrO], shown in Figure 4, that can be loosely described with a linear fit. If it
543 were the case that the gas-phase Br chain length was relatively long (such that the numerator far
544 outweighs the denominator), and dominated by the BrO self-reaction, the numerator in Equations

5 and 6 would reduce to $2k[BrO]^2$, and the regression in Figure 4 would display a quadratic fit; however, that is not observed here.

For purposes of comparison, the chain lengths for Cl and I were also calculated in a manner analogous to that of Equation 5. These results are shown as hourly averages in Figure 5 for the Base with Iodine scenario. It is apparent from this figure that reactive chlorine exhibits an exceptionally short chain length, whereas reactive iodine has a relatively long chain length. The average Cl chain length across the three days of background ozone (25, 29, and 30 March) is 0.15, or 0.23 considering only mid-day hours (12:00 – 18:00 AKST). This result indicates that nearly all Cl atoms that are produced terminate, likely through the very efficient reaction with a multitude of VOCs, as shown in Thompson et al. (2015). This behavior also helps explain why Cl has only a small effect on the bromine chain length. In contrast, I and IO have few known sinks, which results in a reactive iodine chain length of 5.7 on average over 25, 29, and 30 March, and 7.3 over only mid-day hours, with maxima over 12. The high efficiency of the gas-phase regeneration of I in part explains why iodine is more efficient on a per atom basis at depleting ozone than either Br or Cl (Thompson et al., 2015).

3.3 Reactive bromine initiation, propagation, and termination pathways

The individual reactions that initiate, propagate, and terminate the reactive bromine chain were examined to determine the most important reaction pathways contributing the chain reaction. The rates of Br atom production from the most important initiation pathways are shown as hourly averages in Figure 6, with the y-axes expressed as the cumulative rate of reaction, including all five precursors. These are reactions that produce Br atoms from stable reservoir species, which is an important distinction from the propagation reactions that produce

568 Br atoms through radical reactions. Br_2 photolysis is calculated as 2 x $J_{Br2}[Br_2]$. Here, we do not
569 separate Br_2 produced in the gas-phase versus that directly emitted from a surface (this will be
570 discussed further in Section 3.5). The contribution of Br_2 photolysis in producing Br atoms vastly
571 dominates the cumulative production rate (Figure 6A). Therefore, in Figure 6B we show the
572 initiation terms without Br_2 photolysis so that these other production pathways can be visualized.
573 Effectively, Br_2 photolysis alone controls the production of bromine atoms, while the
574 remaining initiation pathways combined add only a minor contribution. Among the minor
575 pathways, HOBr photolysis is the most significant during non-ODE days, with the exception of
576 the high NO_x period of March 25, where $BrNO_2$ has the largest impact. In a highly polluted
577 environment, halogen cycling through NO_x reservoirs would become significantly more
578 important, as has been observed with $ClNO_2$ in mid-latitude regions (Thornton et al., 2010;
579 Mielke et al., 2011; Young et al., 2012). The small contribution of HOBr photolysis to bromine
580 atom production is an important point, because the gas-phase BrO + HOBr ozone depletion cycle
581 (that proceeds via HOBr photolysis rather than surface deposition) has been considered to be
582 significant previously (see, e.g., Hausmann and Platt, 1994), though Zeng et al. (2006) note that
583 HOBr photolysis has only a small effect on BrO_x cycling. Using the version of our model that is
584 unconstrained to HOBr, but incorporates a larger surface deposition in order to reproduce
585 observations (Figure 2C), we were able to determine that photolysis accounts for 19% of the
586 HOBr sink integrated over the 7-day simulation period. Surface deposition accounts for 80%,
587 and other known gas-phase reactions (HOBr + Br, HOBr + Cl, HOBr + OH, HOBr + O) are only
588 minor sink terms at a combined 1%. This corroborates the work of Zeng et al. (2006).
589 The cumulative rates of reaction of the most important propagation pathways, with and
590 without iodine, are shown in Figure 7 A and B. The rate of the BrO + BrO reaction is calculated

591 as $2k[BrO]^2$, since this reaction results in the production of two Br atoms. The reaction pathways
592 that dominate the bromine propagation, i.e., BrO photolysis and reaction with NO, are those that
593 do not result in a net ozone loss. This has been previously recognized and applied to Br steady-
594 state calculations in several works (e.g., Platt and Janssen, 1995; Zeng et al., 2006; Holmes et al.,
595 2010), and demonstrates that much of the time BrO regenerates Br without a net loss of ozone
596 for the simulated conditions in Barrow. Indeed, in our previous paper, we calculated that ~70%
597 of gas-phase BrO reforms ozone via photolysis or reaction with NO over this period (Thompson
598 et al., 2015). The inset pie charts, which show the average fractional importance of the various
599 propagation reactions for 29 and 30 March, reveal that these two pathways account for 84 – 91%
600 of the total. Interestingly, the BrO self-reaction is small in comparison, with an average
601 contribution of 5 – 6%, and a maximum of 46%. However, if we consider only those reactions
602 that *do* lead to a net ozone loss, then the BrO self-reaction accounts for an average of 71% and a
603 maximum of 98% of the propagation. The rate of the BrO + ClO reaction rate is much smaller
604 than that for BrO + BrO, though not insignificant. While on average this reaction pathway
605 accounts for only 2%, it does reach 16% when Cl_2 is high on 29 March. In considering only
606 those reactions that result in a net ozone loss, the BrO + ClO pathway accounts for 21% on
607 average, and up to a maximum of 57%. In Panel B, the Base with Iodine scenario is shown. At
608 these levels, the BrO + IO reaction contributes 4%, which is at times comparable to BrO + BrO
609 and greater than BrO + ClO, even at the low IO mixing ratios in this simulation (~1 pptv).
610 The short gas-phase chain length calculated for bromine propagation indicates that there
611 are large reactive bromine (BrO_x) sinks terminating the chain reaction. Figure 8 presents the
612 rates of the most important BrO_x termination reactions, with the y-axis expressed as the
613 cumulative rate of reaction. Here it can be seen that reaction of BrO with NO_2 is the dominant

614 sink for BrO_x on non-ODE days for the conditions encountered at Barrow, while Br reaction with
615 CH_3CHO is most important when O_3 is depleted. That HO_2 is a significant sink, and would be
616 more so in less anthropogenically-impacted Polar Regions, points toward the importance of
617 heterogeneous recycling through the bromine explosion mechanism. During ozone depletion,
618 such as the major event from days 26 – 28 March ($[O_3] < 5$ppbv) when BrO is mostly absent,
619 CH_3CHO becomes the primary sink term for Br, and HCHO is relatively more important. The
620 strength of the CH_3CHO sink is much greater than is HCHO, as noted previously by Shepson et
621 al. (1996) and Bottenheim et al. (1990). Of note are the relatively similar magnitudes for the
622 total rate of reaction of the initiation, propagation, and termination reactions shown in Figures 6,
623 7, and 8, respectively, which of course must be the case for a chain length near 1. This accounts
624 for the short bromine chain length determined here and also indicates that to sustain elevated
625 bromine radical concentrations necessary to deplete O_3 requires a relatively large Br_2 source,
626 likely in the form of a significant flux of Br_2 from the snow surface, or from in-situ production
627 from aerosols.
628
629 **3.4 Ozone loss rate**
630 Since the chain length calculations seem to suggest a larger than expected contribution of
631 heterogeneous bromine recycling to Br atom production, to examine this further, we calculated
632 the rate of net ozone loss by Br and Cl in the Base Model using Equation 7 and compared this
633 rate to that using the estimation method presented in previous works as shown in Equation 2
634 (Platt and Janssen, 1995; Le Bras and Platt, 1995). Additionally, the total simulated chemical
635 ozone loss in the Base Model was calculated from Equation 8, which includes O_3 destruction by
636 OH, HO_2, and photolysis (determined here as $k[O(^1D)][H_2O]$).

$$O_3 \text{ Loss by Br and Cl} = (k[Br][O_3] - J[BrO] - k[BrO][NO]) + (k[Cl][O_3] - J[ClO] - k[ClO][NO]) \quad (7)$$

$$\text{Total Chemical } O_3 \text{ loss rate} = k[Br][O_3] + k[Cl][O_3] + k[O(^1D)][H_2O] + k[OH][O_3] + k[HO_2][O_3] - k[BrO][NO] - J[BrO] - k[ClO][NO] - J[ClO] \quad (8)$$

The method in Equation 2 assumes that the rate of ozone loss is equivalent to the rate at which Br is regenerated through BrO reaction with itself and ClO (thus assuming efficient gas-phase propagation and a long chain length), whereas Equation 7 accounts for all net ozone destruction by Br and Cl, by correcting for those reactions that release a triplet oxygen atom and reform O_3. In other words, this method accounts for the fact that some BrO radicals react to terminate the chain (and at steady state, an equivalent BrO_x production rate is necessary). Figure 9A compares these two estimations for O_3 loss rate in green (Equation 2) and pink (Equation 7). This comparison clearly shows that there is a large difference between the methods, with the estimation from Equation 2 significantly smaller overall. Additionally, the total chemical O_3 loss (calculated by Equation 8) is shown in the dashed black trace. The O_3 loss rate estimation presented in Equation 7 accounts for nearly all of the chemical O_3 loss (i.e., most chemical O_3 loss is a result of halogen chemistry), such that the dashed black line lies nearly perfectly on top of the pink shaded regions.

In Figure 9B, we show a regression of the two estimation methods (Equation 2 in green and Equation 7 in pink) versus the total chemical O_3 loss rate (Equation 8). Here it can be seen from the pink data that halogen chemistry accounts for 99% of the total chemical O_3 loss under the conditions simulated here. Importantly, the O_3 loss rate estimation presented in Equation 2 accounts for only 44% of the total chemical O_3 loss rate.

In the 1994 work by Hausmann and Platt, the authors also considered the BrO + HO gas-phase ozone depletion cycle as a proxy for estimating the O_3 loss rate, using the equation shown below (Equation 17 of Hausmann and Platt, 1994).

$$-\frac{d[O_3]}{dt} = (k_5 \cdot [BrO] \cdot [HO_2]) \quad (9)$$

The authors only considered the gas-phase cycle of HOBr here with the photolysis of HOBr regenerating Br. At the time of this publication, the heterogeneous cycling of HOBr had only recently been proposed and had not been fully validated. Hausmann and Platt showed that Equation 9 resulted in a significantly lower estimation for O_3 depletion than did Equation 1, which considered only the BrO-BrO cycle. In Figure 9B, we show also the O_3 loss rate estimated using Equation 9 in blue. Our results corroborate that of Hausmann and Platt (1994), and demonstrate that Equation 9 can account for only 18% of the O_3 loss. This is also supported by our results discussed previously that show that only 19% of HOBr is lost to photolysis. To examine this one step further, we present an additional regression in Figure 8B (orange trace) that combines Equations 2 and 9, thereby considering the three predominant gas-phase O_3 depletion cycles of BrO-BrO, BrO-ClO, and BrO-HO_2. This still can only account for 60% of the O_3 loss.

Our analysis quantitatively expresses the conclusion that the gas-phase recycling of bromine is not as efficient as previously considered and that it is often the case, for Barrow, that BrO_x terminations must often, through reactions R5 or R10, be followed by heterogeneous production of Br_2 through condensed-phase reactions of HOBr and/or $BrONO_2$. An important conclusion from this analysis is that the chemical O_3 loss rate is largely underestimated when calculated from only BrO observations using the previously accepted $2(k[BrO]^2 + [BrO][ClO])$ method, and one should be cautious about drawing conclusions about O_3 depletion rates and

683 timescales based solely on BrO observations. This may have significant impacts on the process
684 of examining ODEs and addressing the extent to which they represent local scale chemistry
685 versus transport effects. While this situation is significantly impacted by local NO_x sources at
686 Barrow, NO_x is expected to increase with development around the Arctic.
687
688 **3.5 Bromine atom production**
689 If it is the case that heterogeneous recycling is of such importance, it may be that
690 Reaction R5 (BrO + HO_2) competes favorably with Reaction R3 (BrO + BrO). Panel A of
691 Figure 10 shows the rates of reactions R5 and R3. This plot demonstrates that for our modeling
692 results the rate of reaction of BrO with HO_2 is often of a comparable or greater magnitude than
693 the BrO self-reaction, and remains significant throughout the simulated period. Previous
694 modeling work by Sander et al. (1997) also compared the rates of these two critical reactions
695 (Figure 2 of that work). In contrast to our results, their model predicted that the rate of the BrO +
696 BrO reaction was up to a factor of 8 greater than that of BrO + HO_2. The reason for this
697 difference may perhaps be the much lower mixing ratios of HO_2 in the model by Sander and
698 coworkers. Their model predicted HO_2 daily maxima of 0.2 to 0.6 pptv for most days, increasing
699 to 1.8 pptv on the final three days of their simulation. In contrast, HO_2 observations at Barrow
700 were frequently greater than 5 pptv and up to 10 pptv. As demonstrated in Thompson et al.
701 (2015), HCHO was a dominant factor in controlling the HO_2 mixing ratios in Barrow. The low
702 levels of HO_2 in Sander et al. (1997) likely also contribute to their low predicted HOBr mixing
703 ratios, which do not exceed 1 pptv in their model. This also is much lower than observations at
704 Barrow, where HOBr reaching 10 pptv to 20 pptv was measured during our simulated period.
705 Because the BrO + HO_2 reaction is of primary importance for the bromine explosion mechanism,

706 our result supports the hypothesis that heterogeneous recycling may be equally or even more
707 important than gas-phase recycling of reactive bromine.

708 Given that the chain length is small, it must be that initiation is an important source of Br
709 atoms in order to sustain BrO and lead to O_3 depletion. To further examine the question of
710 surface emissions versus gas-phase recycling, we determined the rate of production of Br atoms
711 via photolysis of Br_2 and BrCl (Equation 10) compared to the rate of production of Br atoms
712 through gas-phase recycling calculated by Equation 11. Because our model is constrained by Br_2
713 observations and we do not produce Br_2 from surfaces via heterogeneous reactions, the
714 photolysis of Br_2 includes Br_2 that is both emitted from surfaces and that is formed via gas-phase
715 reactions. To correct for the Br_2 that is formed in the gas-phase reactions so that Equation 10
716 represents our best approximation for surface-emitted Br_2, we created a proxy in the model, Br_2*,
717 that represents the Br_2 produced from gas phase reactions. These reactions include Br + $BrNO_2$,
718 Br + $BrONO_2$, and the BrO + BrO branch that produces Br_2. Equation 10 is thus corrected for the
719 gas-phase generated Br_2 by subtracting the photolysis of Br_2*. A comparison of Br_2 and Br_2*
720 reveals that these three gas-phase production pathways account for an average of 35% of
721 observed Br_2, suggesting that the snowpack and/or aerosols emits the remaining 65%. Again, we
722 cannot distinguish between snow or aerosol production using this method.

723

724 $$\textit{Br Production from Surface-derived } Br_2\textit{, BrCl} = 2 \times J_{Br2}[Br_2] + J_{BrCl}[BrCl] - 2 \times J_{Br2}[Br_2^*] \quad (10)$$

725

726

727 $$\textit{Br Production via Gas-phase Recycling} = 2k[BrO][BrO] + k[BrO][ClO] \quad (11)$$
728 $$+ k[BrO][NO] + k[BrO][OH] + k[BrO][O(^3P)]$$
729 $$+ k[BrO][CH_3OO] + k[BrO][CH_3COOO]$$
730 $$+ J_{HOBr}[HOBr] + J_{BrO}[BrO] + J_{BrONO2}[BrONO_2]$$
731 $$+ J_{BrNO2}[BrNO_2]$$

732

733 Panel B of Figure 10 compares the results of Equations 10 and 11, showing the total rate of Br
734 atom production separated into Br production from the derived "surface-emitted" Br_2 and BrCl
735 (purple) and from gas-phase Br recycling (orange); Panel C plots the fraction of total Br atom
736 production that is due to production from Br_2 and BrCl surface emissions. The majority of the
737 time during this 7-day period Br atom production from Br_2 and BrCl emissions (Equation 10)
738 accounts for 30% or greater of the total, and at times reaches up to 90%. This explains both how
739 ozone depletion can be rapid despite the short calculated bromine radical chain length, as well as
740 the difference found between the two methods of estimating O_3 loss rate in Figure 9. It is
741 concluded from this analysis, then, that the condensed phase recycling of bromine can be of
742 equal or greater importance to the evolution of ODEs than gas-phase Br regeneration through
743 radical recycling reactions.
744
745 **4 Conclusions**
746 The analysis presented here suggests that the gas-phase recycling of bromine species may
747 be less important than commonly believed, and we conclude that heterogeneous recycling is
748 critical for the evolution of ODEs/AMDEs, consistent with results by Michalowski et al. (2000),
749 Piot and von Glasow (2008), and Toyota et al. (2011, 2014). To support this conclusion, we have
750 used the gas-phase bromine chain length, which has not previously been applied to Arctic
751 halogen chemistry, as an objective metric. The gas-phase bromine chain length is much shorter
752 than expected, suggesting that much of the Br present in the gas-phase is Br from surface
753 emissions. Again note that our calculation of chain length includes photolysis of BrO and BrO +
754 NO, which do not result in net O_3 loss. Had we omitted these two reactions, which we have
755 found are in fact dominating the radical propagation, the chain length would be, on average, 80%
756 shorter. Because of the small chain length calculated for Br, one must be cautious about drawing

conclusions about O_3 depletion from BrO measurements alone. We recommend concurrent measurements of a broad suite of inorganic bromine species for accurate study of these ozone depletion events. The very low mixing ratios of HOBr predicted by Sander et al. (1997) and the high mixing ratios originally predicted by our model point to the need for measurements of these species to validate the accuracy of Arctic models.

We find that between 30 – 90% of Br atoms are produced from surface emissions of Br_2 and BrCl, though we cannot distinguish snow sources from aerosol sources using our model. However, it is important to note that we do not know how much of the condensed phase Br_2 production derives from reaction R7, or from some other condensed phase process, e.g. oxidation of Br^- by OH radicals (Abbatt et al., 2010). The in situ snow chamber experiments by Pratt et al. (2013) demonstrate a strong Br_2 source from the snowpack; similar field observations proving significant Br_2 emissions from Arctic aerosol are currently lacking. If the snow surface is the primary sources of these emissions, then a strong vertical gradient would be expected in the near surface boundary layer, and our estimations for the Br chain length would be only valid for the height of our measurements (~ 1 m above the snow). Strong deposition to the snow would also induce a vertical gradient in these species. If, however, aerosols are an important source of Br_2 (or other halogen precursors), then Br_2 production should occur throughout the entire height of the boundary with no significant vertical gradient, in a similar fashion as has been observed for $ClNO_2$, which is a known product of aerosol chemistry (Young et al., 2012). It is clear that vertically-resolved measurements of these halogen precursors are imperative for our understanding of halogen production in the Arctic.

The production of Br_2 is quite complex and is dependent on many factors, including the relative concentrations of bromide and chloride (among others), the availability of atmospheric

780 oxidants, such as ozone (e.g., Oum et al., 1998; Pratt et al., 2013), the pH of the snow surfaces or
781 aerosol (Toyota et al., 2011, 2014), the presence of snow phase oxidants such as H_2O_2 (Pratt et
782 al., 2013), and the replenishment of the snowpack halides from deposited sea salts. The last of
783 these is governed by meteorology, the proximity of open water or saline sea ice surfaces, and
784 wind/storm events, making the accurate modeling of these processes very complex (Domine et
785 al., 2013). Likewise, to date, it has not been possible to determine the halide concentrations or
786 pH of the snow grain surfaces, and these values are likely highly variable and dependent on snow
787 and aerosol aging and deposition of atmospheric constituents. Due to the apparent importance of
788 surface chemistry for both the initiation and evolution of Arctic ozone depletion events, it is clear
789 that more laboratory and field studies are required to decipher these complex chemical and
790 physical processes. In particular, we strongly recommend studies relating to direct
791 measurements of surface fluxes of molecular halogens, as a function of conditions of temperature,
792 snowpack composition, and pH, as well as deposition velocities for the hypohalous acids (HOBr,
793 HOCl) to the snow. Our model overestimation of HOBr, that necessitated constraint to
794 observations, suggests a sometimes much stronger, but also variable, deposition of HOBr that is
795 currently unknown. Further, there is currently little understanding of the mechanism for Cl_2
796 production in the Arctic, and no successful measurements of IO in the High Arctic. Recent
797 observations of I_2 within the Barrow snowpack (Raso et al., 2016) suggest reactive iodine
798 chemistry is present in this region, and this would have an impact on Br recycling and ozone
799 depletion rate. Investigations into these areas would greatly increase our understanding of
800 halogen chemistry and ozone depletion in the Arctic.
801

Acknowledgements This work was funded by the National Science Foundation grant ARC-0732556. Partial support for CT during preparation of this manuscript was provided by the NSF Atmospheric and Geospace Sciences Postdoctoral Research Fellowship program. The authors wish to thank the organizers of the OASIS 2009 field campaign, the Barrow Arctic Science Consortium for logistics support, and all of the researchers who contributed to the campaign. This paper is submitted in memory of our colleague and friend, Roland von Glasow.

References

Abbatt, J., Oldridge, N., Symington, A., Chukalovskiy, V., McWhinney, R. D., Sjostedt, S. and Cox, R. A.: Release of Gas-Phase Halogens by Photolytic Generation of OH in Frozen Halide−Nitrate Solutions: An Active Halogen Formation Mechanism?, J. Phys. Chem. A, 114(23), 6527–6533, doi:10.1021/jp102072t, 2010.

Abbatt, J. P. D., Thomas, J. L., Abrahamsson, K., Boxe, C., Granfors, A., Jones, A. E., King, M. D., Saiz-Lopez, A., Shepson, P. B., Sodeau, J., Toohey, D. W., Toubin, C., von Glasow, R., Wren, S. N., and Yang, X.: Halogen activation via interactions with environmental ice and snow in the polar lower troposphere and other regions, Atmos. Chem. Phys., 12, 6237-6271, 2012.

Adams, J., Holmes, N., and Crowley, J.: Uptake and reaction of HOBr on frozen and dry NaCl/NaBr surfaces between 253 and 233K, Atmos. Chem. Phys., 2, 79 – 91, doi: 10.5194/acp-2-79-2002, 2002.

Ariya, P., Jobson, B., Sander, R., Niki, H., Harris, G., Hopper, J., and Anlauf, K.: Measurements of C2-C7 hydrocarbons during the Polar Sunrise Experiment 1994: Further evidence for halogen chemistry in the troposphere, J. Geophys. Res., 103, 13169-13180, 1998.

Atkinson, R., Baulch, D. L., Cox, R. A., Crowley, J. N., Hampson, R. F., Hynes, R. G., Jenkin, M. E., Rossi, M. J. and Troe, J.: Evaluated kinetic and photochemical data for atmospheric chemistry: Volume II gas phase reactions of organic species, Atmos. Chem. Phys., 6, 3625-4055, 2006.

Atkinson, R., Baulch, D. L., Cox, R. A., Crowley, J. N., Hampson, R. F., Hynes, R. G., Jenkin, M. E., Rossi, M. J. and Troe, J.: Evaluated kinetic and photochemical data for atmospheric chemistry: Volume III gas phase reactions of inorganic halogens, Atmos. Chem. Phys., 7, 981-119, 2007.

Barrie, L., Bottenheim, J., Schnell, R., Crutzen, P., and Rasmussen, R.: Ozone destruction and photochemical reactions at polar sunrise in the lower Arctic atmosphere, Nature, 334, 138 - 141, doi: 10.1038/334138a0, 1988.

Bottenheim, J.W., Barrie, L. A., Atlas, E., Heidt, L. E., Niki, H., Rasmussen, R. A., and Shepson, P.B.: Depletion of lower tropospheric ozone during Arctic spring: The Polar Sunrise Experiment 1998, J. Geophys. Res., 95, 18555-18568, 1990.

Calvert, J. G., and Lindberg, S. E.: Potential influence of iodine-containing compounds on the chemistry of the troposphere in the polar spring. I. Ozone depletion, Atmos. Environ., 38, 5087-5104, doi: 10.1016/j.atmosenv.2004.05.049, 2004.

Cao, L., Sihler, H., Platt, U., and Gutheil, E.: Numerical analysis of the chemical kinetic mechanisms of ozone depletion and halogen release in the polar troposphere, Atmos. Chem. Phys., 14, 3771-3787, 2014.

Carpenter, L. J., S. M. MacDonald, M. D. Shaw, R. Kumar, R.W. Saunders, R. Parthipan, J.Wilson and J. M. C. Plane, Atmospheric iodine levels influenced by sea surface emissions of inorganic iodine, Nature Geosci*., 6,* 108-111, doi: 10.1038/ngeo1687, 2013.

Cavender, A., Biesenthal, T., Bottenheim, J., and Shepson, P.: Volatile organic compound ratios as probes of halogen atom chemistry in the Arctic, Atmos. Chem. Phys., 8, 1737-1750, 2008.

Custard, K. D., Thompson, C. R., Pratt, K. A., Shepson, P. B., Liao, J., Huey, L. G., Orlando, J. J., Weinheimer, A. J., Apel, E., Hall, S. R., Flocke, F., Mauldin, L., Hornbrook, R. S., Pöhler, D., General, S., Zielcke, J., Simpson, W. R., Platt, U., Fried, A., Weibring, P., Sive, B. C., Ullmann, K., Cantrell, C., Knapp, D. J., and Montzka, D. D.: The NOx dependence of bromine chemistry in the Arctic atmospheric boundary layer, Atmos. Chem. Phys., 15, 10799-10809, 2015.

Domine, F., J. Bock, D. Voisin, and D. J. Donaldson, Can We Model Snow Photochemistry? Problems with the Current Approaches, J. Phys. Chem., A*,* 117, 4733−4749, doi: 10.1021/jp3123314, 2013.

Edwards, G. D., Cantrell, C. A., Stephens, S., Hill, B., Goyea, O., Shetter, R. E., Mauldin III, R. L., Kosciuch, E., Tanner, D. J., and Eisele, F. L.: Chemical ionization mass spectrometer instrument for the measurement of tropospheric HO_2 and RO_2, Anal. Chem., 75, 5317-5327, doi: 10.1021/ac034402b, 2003.

Ehhalt, D. H.: Photooxidation of trace gases in the troposphere Plenary Lecture, Phys. Chem. Chem. Phys., 1, 5401-5408, 1999.

Fan, S-M. and D. J. Jacob, Surface ozone depletion in Arctic spring sustained by bromine reactions on aerosols, Nature, 358*,* 522-524, 1992.

Foster, K. L., Plastridge, R. A., Bottenheim, J. W., Shepson, P. B., Finlayson-Pitts, B. J., and Spicer, C. W.: The role of Br_2 and BrCl in surface ozone destruction at polar sunrise, Science, 291, 471-474, 2001.

Frieß, U., Deutschmann, T., Gilfedder, B., Weller, R., and Platt, U.: Iodine monoxide in the Antarctic snowpack, Atmos. Chem. Phys, 10, 2439-2456, 2010.

Gladich, I., J. S. Francisco, R. J. Buszek, M. Vazdar, M. A. Caignano, and P. B. Shepson, *Ab Initio* Study of the Reaction of Ozone with Bromide Ion, J. Phys. Chem. A, 119, 4482−4488, 2015.

Gong, S., Walmsley, J., Barrie, L., and Hopper, J.: Mechanisms for surface ozone depletion and recovery during polar sunrise, Atmos. Environ., 31, 969-981, 1997.

Guimbaud, C., Grannas, A. M., Shepson, P. B., Fuentes, J. D., Boudries, H., Bottenheim, J. W., Dominé, F., Houdier, S., Perrier, S., and Biesenthal, T. B.: Snowpack processing of acetaldehyde and acetone in the Arctic atmospheric boundary layer, Atmos. Environ., 36, 2743-2752, 2002.

Hausmann, M., and Platt, U.: Spectroscopic measurement of bromine oxide and ozone in the high Arctic during Polar Sunrise Experiment 1992, J. Geophys. Res., 99, 25399, 1994.

Helmig, D., Ganzeveld, L., Butler, T., and Oltmans, S.: The role of ozone atmosphere-snow gas exchange on polar, boundary-layer tropospheric ozone? a review and sensitivity analysis, Atmos. Chem. Phys., 7, 15-30, 2007.

Helmig, D., Boylan, P., Johnson, B., Oltmans, S., Fairall, C., Staebler, R., Weinheimer, A., Orlando, J., Knapp, D. J., Montzka, D. D., Flocke, F., Frieß, U., Sihler, H., and Shepson, P. B.: Ozone dynamics and snow-atmosphere exchanges during ozone depletion events at Barrow, Alaska, J. Geophys. Res., 117, D20303, doi:10.1029/2012JD017531, 2012.

Hirokawa, J., Onaka, K., Kajii, Y., and Akimoto, H.: Heterogeneous processes involving sodium halide particles and ozone: molecular bromine release in the marine boundary layer in the absence of nitrogen oxides, Geophys. Res. Lett., 25, 2449-2452, 1998.

Holmes, C. D., Jacob, D. J., Corbitt, E. S., Mao, J., Yang, X., Talbot, R., and Slemr, F.: Global atmospheric model for mercury including oxidation by bromine atoms, Atmos. Chem. Phys., 10, 12037-12057, 2010.

Hönninger, G.: Halogen Oxide Studies in the Boundary Layer by Multi Axis Differential Optical Absorption Spectroscopy and Active Longpath-DOAS, Ph.D., University of Heidelberg, 2002.

Huff, A. K., and Abbatt, J. P. D.: Kinetics and product yields in the heterogeneous reactions of HOBr with ice surfaces containing NaBr and NaCl, J. Phys. Chem. A, 106, 5279-5287, 2002.

Jacob, D. J.: Heterogeneous chemistry and tropospheric ozone, Atmos. Environ., 34, 2131-2159, 2000.

930 Jobson, B., Niki, H., Yokouchi, Y., Bottenheim, J., Hopper, F., and Leaitch, R.: Measurements
931 of C2-C6 hydrocarbons during the Polar Sunrise 1992 Experiment: Evidence for Cl atom and Br
932 atom chemistry, J. Geophys. Res., 99, 25355-25368, 1994.
933
934 Kukui, A., Kirchner, U., Benter, T., and Schindler, R. N.: A gas kinetic investigation of HOBr
935 reactions with Cl(^{2}P), O(^{3}P) and OH(^{2}II). The reaction of BrCl with OH(^{2}II), Berichte Der
936 Bunsen-Gesellschaft-Physical Chemistry Chemical Physics, 100, 455-461, 1996.
937
938 Kuo, K. K.: Principles of combustion, John Wiley & Sons, New York, 1986.
939
940 Lary, D.: Gas phase atmospheric bromine photochemistry, J. Geophys. Res., 101, 1505-1516,
941 1996.
942
943 Le Bras, G., and Platt, U.: A possible mechanism for combined chlorine and bromine catalyzed
944 destruction of tropospheric ozone in the Arctic, Geophys. Res. Lett., 22, 599-602, 1995.
945
946 Lehrer, E., Hönninger, G., and Platt, U.: A one dimensional model study of the mechanism of
947 halogen liberation and vertical transport in the polar troposphere, Atmos. Chem. Phys., 4, 2427-
948 2440, 2004.
949
950 Liao, J., Huey, L., Scheuer, E., Dibb, J., Stickel, R., Tanner, D., Neuman, J., Nowak, J., Choi, S.,
951 and Wang, Y.: Characterization of soluble bromide measurements and a case study of BrO
952 observations during ARCTAS, Atmos. Chem. Phys, 12, 1327-1338, 2012a.
953
954 Liao, J., Huey, L., Tanner, D., Flocke, F., Orlando, J., Neuman, J., Nowak, J., Weinheimer, A.,
955 Hall, S., Smith, J., Fried, A., Staebler, R., Wang, Y., Koo, J.-H., Cantrell, C., Weibring, P.,
956 Walega, J., Knapp, D., Shepson, P., and Stephens, C.: Observations of inorganic bromine (HOBr,
957 BrO, and Br_2) speciation at Barrow, Alaska, in spring 2009, J. Geophys. Res., 117, D00R16,
958 2012b.
959
960 Liao, J., L. G. Huey, Z. Liu, D. J. Tanner, C. A. Cantrell, J. J. Orlando, F. M. Flocke, P. B.
961 Shepson, A. J. Weinheimer, S. R. Hall, H. J. Beine, Y. Wang, E. D. Ingall, C. R. Stephens, R. S.
962 Hornbrook, E. Apel, A. Fried, L. Mauldin, J. N. Smith, R. M. Staebler, J.A. Neuman, J.B.
963 Nowak, High levels of molecular chlorine in the Arctic atmosphere, Nature Geosci., 7, 91 – 94,
964 doi:10.1038/ngeo2046, 2014.

965 Mahajan, A., Shaw, M., Oetjen, H., Hornsby, K., Carpenter, L., Kaleschke, L., Tian-Kunze, X.,
966 Lee, J., Moller, S., and Edwards, P.: Evidence of reactive iodine chemistry in the Arctic
967 boundary layer, J. Geophys. Res., 115, D20303, doi: 10.1029/2009JD013665, 2010.
968
969 Mallard, W. G., Westley, F., Herron, J. T., Hampson, R. F., and Frizzel, D. H.: NIST Chemical
970 Kinetics Database: Version 5.0 National Institute of Standards and Technology, Gaithersburg,
971 MD. , 1993.

972

973 Martinez, M., Arnold, T., and Perner, D.: The role of bromine and chlorine chemistry for arctic
974 ozone depletion events in Ny-Ålesund and comparison with model calculations, Annales
975 Geophysicae, 17, 941-956, 1999.
976
977 McFiggans, G., Plane, J. M. C., Allan, B. J., Carpenter, L. J., Coe, H., and O'Dowd, C.: A
978 modeling study of iodine chemistry in the marine boundary layer, J. Geophys. Res., 105, 14371-
979 14385, 2000.
980
981 McFiggans, G., Cox, R. A., Mössinger, J. C., Allan, B. J., and Plane, J. M. C.: Active chlorine
982 release from marine aerosols: Roles for reactive iodine and nitrogen species, J. Geophys. Res,
983 107, doi: 10.1029/2001JD000383, 2002.
984
985 Michalowski, B. A., Francisco, J. S., Li, S. M., Barrie, L. A., Bottenheim, J. W., and Shepson, P.
986 B.: A computer model study of multiphase chemistry in the Arctic boundary layer during polar
987 sunrise, J. Geophys. Res., 105, 15131 – 15145, 2000.
988
989 Mielke, L. H., Furgeson, A., and Osthoff, H. D.: Observation of $ClNO_2$ in a mid-continental
990 urban environment, Environ. Sci. Technol., 45, 8889-8896, 2011.
991
992 Monks, P. S.: Gas-phase radical chemistry in the troposphere, Chem. Soc. Rev., 34, 376-395,
993 2005.
994
995 Neuman, J. A., Nowak, J. B., Huey, L. G., Burkholder, J. B., Dibb, J. E., Holloway, J. S., Liao, J.,
996 Peischl, J., Roberts, J. M., Ryerson, T. B., Scheuer, E., Stark, H., Stickel, R. E., Tanner, D. J.,
997 and Weinheimer, A.: Bromine measurements in ozone depleted air over the Arctic Ocean, Atmos.
998 Chem. Phys., 10, 6503-6514, 2010.
999
1000 Oum, K., Lakin, M., DeHaan, D., Brauers, T., and Finlayson-Pitts, B.: Formation of molecular
1001 chlorine from the photolysis of ozone and aqueous sea-salt particles, Science, 279, 74, 1998a.
1002
1003 Oum, K., Lakin, M., and Finlayson-Pitts, B.: Bromine activation in the troposphere by the dark
1004 reaction of O_3 with seawater ice, Geophys. Res. Lett., 25, 3923-3926, 1998b.
1005
1006 Papanastasiou, D.K., McKeen, S. A., and Burkholder, J. B.: The very short-lived ozone depleting
1007 substance CHBr3 (bromoform): revised UV absorption spectrum, atmospheric lifetime, and
1008 ozone depletion potential, Atmos. Chem. Phys., 14, 3017 – 3025, 2014.
1009
1010 Piot, M., and Von Glasow, R.: The potential importance of frost flowers, recycling on snow, and
1011 open leads for ozone depletion events, Atmos. Chem. Phys., 8, 2437-2467, 2008.
1012
1013 Platt, U., and Janssen, C.: Observation and role of the free radicals NO_3, ClO, BrO and IO in the
1014 troposphere, Faraday Discuss., 100, 175-198, 1995.
1015
1016 Pöhler, D., Vogel, L., Frieß, U., and Platt, U.: Observation of halogen species in the Amundsen
1017 Gulf, Arctic, by active long-path differential optical absorption spectroscopy, Proceedings of the
1018 National Academy of Sciences, 107, 6582, 2010.

Pratt, K. A., Custard, K. D., Shepson, P. B., Douglas, T. A., Pöhler, D., General, S., Zielcke, J., Simpson, W. R., Platt, U., Tanner, D. J., Huey, L. G., Carlsen, M., and Stirm, B. H.: Photochemical production of molecular bromine in Arctic surface snowpacks, Nature Geosci., 6, 351 – 356, doi: 10.1038/ngeo1779, 2013.

Raso, A. R. W., Custard, K. D., Pratt, K. A., Tanner, D. J., Huey, L. G., and Shepson, P. B.: Active molecular iodine snowpack photochemistry in the Arctic, Proc. Nat. Acad. Sci., submitted, 2016.

Saiz-Lopez, A., Mahajan, A. S., Salmon, R. A., Bauguitte, S. J. B., Jones, A. E., Roscoe, H. K., and Plane, J. M. C.: Boundary layer halogens in coastal Antarctica, Science, 317, 348-351, 2007.

Saiz-Lopez, A., Plane, J. M. C., Mahajan, A. S., Anderson, P. S., Bauguitte, S. J. B., Jones, A. E., Roscoe, H. K., Salmon, R. A., Bloss, W. J., and Lee, J. D.: On the vertical distribution of boundary layer halogens over coastal Antarctica: implications for O_3, HO_x, NO_x and the Hg lifetime, Atmos. Chem. Phys., 8, 887-900, 2008.

Sander, R., Keene, W. C., Pszenny, A. A. P., Arimoto, R., Ayers, G. P., Baboukas, E., Cainey, J. M., Crutzen, P. J., Duce, R. A., Hönninger, G., Huebert, B. J., Maenhaut, W., Mihalopoulos, N., Turekian, C., and van Dingenen, R.: Inorganic bromine in the marine boundary layer: a critical review, Atmos. Chem. Phys., 3, 1301-1336, 2003.

Shetter, R. E., and Müller, M.: Photolysis frequency measurements using actinic flux spectroradiometry during the PEM-Tropics mission: Instrumentation description and some results, J. Geophys. Res., 104, 5647-5661, 1999.

Shepson, P. B., Sirju, A.-P., Hopper, J. F., Barrie, L. A., Young, V., Niki, H. and Dryfhout, H.: Sources and sinks of carbonyl compounds in the Arctic Ocean boundary layer: a polar ice floe experiment, J. Geophys. Res., 101, 21081 - 21089, 1996.

Staebler, R. M., den Hartog, G., Georgi, B., and Sterdiek, T. D.: Aerosol size distribution in Arctic haze during the Polar Sunrise Experiment 1992, J. Geophys. Res., 99, 25429-25437, 1994.

Sumner, A. L., and Shepson, P. B.: Snowpack production of formaldehyde and its effect on the Arctic troposphere, Nature, 398, 230-233, 1999.

Stephens, C. R., Shepson, P. B., Steffen, A., Bottenheim, J. W., Liao, J., Huey, L. G., Apel, E., Weinheimer, A., Hall, S. R., and Cantrell, C.: The relative importance of chlorine and bromine radicals in the oxidation of atmospheric mercury at Barrow, Alaska, J. Geophys. Res., 117, D00R11, doi: 10.1029/2011JD016649, 2012.

Sturges, W., and Barrie, L.: Chlorine, bromine and iodine in Arctic aerosols, Atmos. Environ., 22, 1179-1194, 1988.

Tang, T., and McConnell, J.: Autocatalytic release of bromine from Arctic snow pack during polar sunrise, Geophys. Res. Lett., 23, 2633-2636, 1996.

Thomas, J. L., Stutz, J., Lefer, B., Huey, L. G., Toyota, K., Dibb, J. E., and von Glasow, R.: Modeling chemistry in and above snow at Summit, Greenland – Part 1: Model description and results, Atmos. Chem. Phys., 11, 4899-4914, 2011.

Thompson, C. R., Shepson, P. B., Liao, J., Huey, L. G., Apel, E. C., Cantrell, C. A., Flocke, F., Orlando, J., Fried, A., Hall, S. R., Hornbrook, R. S., Knapp, D. J., Mauldin III, R. L., Montzka, D. D., Sive, B. C., Ullmann, K., Weibring, P. and Weinheimer, A.: Interactions of bromine, chlorine, and iodine photochemistry during ozone depletions in Barrow, Alaska, Atmos. Chem. Phys., 15, 9651 – 9679, doi: 10.5194/acp-15-9651-2015, 2015.

Thornton, J. A., Kercher, J. P., Riedel, T. P., Wagner, N. L., Cozic, J., Holloway, J. S., Dubé, W. P., Wolfe, G. M., Quinn, P. K., Middlebrook, A. M., Alexander, B., and Brown, S. S.: A large atomic chlorine source inferred from mid-continental reactive nitrogen chemistry, Nature, 464, 271-274, 2010.

Toyota, K., McConnell, J. C., Lupu, A., Neary, L., McLinden, C. A., Richter, A., Kwok, R., Semeniuk, K., Kaminski, J. W., Gong, S. –L., Jarosz, J., Chipperfield, M. P., and Sioris, C. E.: Analysis of reactive bromine production and ozone depletion in the Arctic boundary layer using 3-D simulations with GEM-AQ: inference from synoptic-scale patterns, Atmos. Chem. Phys., 11, 3949-3979, 2011.

Toyota, K., McConnell, J. C., Staebler, R. M., and Dastoor, A. P.: Air-snowpack exchange of bromine, ozone and mercury in the springtime Arctic simulated by the 1-D model PHANTAS - Part 1: In-snow bromine activation and its impact on ozone, Atmos. Chem. Phys., 14, 4101-4133, 2014.

Vogt, R., Crutzen, P. J., and Sander, R.: A mechanism for halogen release from sea-salt aerosol in the remote marine boundary layer, Nature, 383, 327 – 330, doi: 10.1038/383327a0, 1996.

Vogt, R., Sander, R., von Glasow, R., and Crutzen, P. J.: Iodine chemistry and its role in halogen activation and ozone loss in the marine boundary layer: A model study, J. Atmos. Chem., 32, 375-395, 1999.

Wennberg, P., Hanisco, T., Jaegle, L., Jacob, D., Hintsa, E., Lanzendorf, E., Anderson, J., Gao, R. S., Keim, E., and Donnelly, S.: Hydrogen radicals, nitrogen radicals, and the production of O_3 in the upper troposphere, Science, 279, 49-53, 1998.

Young, C. J., Washenfelder, R. A., Roberts, J. M., Mielke, L. H., Osthoff, H. D., Tsai, C., Pikelnayai, O., Stutz, J., Veres, P. R., Cochran, A. K., VandenBoer, T. C., Flynn, J., Grossberg, N., Haman, C. L., Lefer, B., Stark, H., Graus, M., de Gouw, J., Gilman, J. B., Kuster, W. C., and Brown, S. S.: Vertically resolved measurements of nighttime radical reservoirs in Los Angeles and their contribution to the urban radical budget, Environ. Sci. Technol., 46, 10965-10973, 2012.

Zeng, T., Wang, Y., Chance, K., Blake, N., Blake, D., and Ridley, B.: Halogen-driven low-altitude O_3 and hydrocarbon losses in spring at northern high latitudes, J. Geophys. Res, 111, D17, doi: 10.1029/2005JD006706, 2006.

Table 1. Reactions used in the model that are pertinent to bromine chemistry. All rate constants (with the exception of photolysis *J* coefficients) are in units of cm^3 $molecule^{-1}$ s^{-1}.

Gas-Phase Reactions	**Rate Constant**	**Reference**
$Br + O_3 \rightarrow BrO$	6.75×10^{-13}	*Atkinson et al.* [2004]
$Br + C_2H_4 \rightarrow HBr + C_2H_5OO$	1.3×10^{-13}	*Atkinson et al.* [2004]
$Br + C_3H_6 \rightarrow HBr + C_3H_5$	1.60×10^{-12}	*Atkinson et al.* [2004]
$Br + HCHO \rightarrow HBr + CO + HO_2$	6.75×10^{-13}	*Sander et al.* [2006]
$Br + CH_3CHO \rightarrow HBr + CH_3COOO$	2.8×10^{-12}	*Atkinson et al.* [2004]
$Br + C_3H_6O \rightarrow HBr$	9.7×10^{-12}	*Wallington et al.* [1989]
Br + nButanal → HBr	9.7×10^{-12}	estimate from *Michalowski et al.* [2000]
$Br + CH_3OOH \rightarrow HBr + CH_3OO$	4.03×10^{-15}	*Mallard et al.* [1993]
$Br + NO_2 \rightarrow BrNO_2$	2.7×10^{-11}	*Atkinson et al.* [2004]
$Br + BrNO_3 \rightarrow Br_2 + NO_3$	4.9×10^{-11}	*Orlando and Tyndall* [1996]
$Br + OClO \rightarrow BrO + ClO$	1.43×10^{-13}	*Atkinson et al.* [2004]
$BrO + O(^3P) \rightarrow Br$	4.8×10^{-11}	*Atkinson et al.* [2004]
$BrO + OH \rightarrow Br + HO_2$	4.93×10^{-11}	*Atkinson et al.* [2004]
$BrO + HO_2 \rightarrow HOBr$	3.38×10^{-11}	*Atkinson et al.* [2004]
$BrO + CH_3OO \rightarrow HOBr + CH_2OO$	4.1×10^{-12}	*Aranda et al.* [1997]
$BrO + CH_3OO \rightarrow Br + HCHO + HO_2$	1.6×10^{-12}	*Aranda et al.* [1997]
$BrO + CH_3COOO \rightarrow Br + CH_3COO$	1.7×10^{-12}	estimate from *Michalowski et al.* [2000]
$BrO + C_3H_6O \rightarrow HOBr$	1.5×10^{-14}	estimate from *Michalowski et al.* [2000]
$BrO + NO \rightarrow Br + NO_2$	2.48×10^{-11}	*Atkinson et al.* [2004]
$BrO + NO_2 \rightarrow BrNO_3$	1.53×10^{-11}	*Atkinson et al.* [2004]
$BrO + BrO \rightarrow Br + Br$	2.82×10^{-12}	*Sander et al.* [2006]
$BrO + BrO \rightarrow Br_2$	9.3×10^{-13}	*Sander et al.* [2006]
$BrO + HBr \rightarrow HOBr + Br$	2.1×10^{-14}	*Hansen et al.* [1999]
$HBr + OH \rightarrow Br + H_2O$	1.26×10^{-11}	*Sander et al.* [2006]
$CH_3Br + OH \rightarrow H_2O + Br$	1.27×10^{-14}	*Atkinson et al.* [2004]
$CHBr_3 + OH \rightarrow H_2O + Br$	1.2×10^{-13}	*Atkinson et al.* [2004]
$Cl + BrCl \leftrightarrow Br + Cl_2$	f: 1.5×10^{-11} r: 1.1×10^{-15}	*Clyne et al.* [1972]
$Cl + Br_2 \leftrightarrow BrCl + Br$	f: 1.2×10^{-10} r: 3.3×10^{-15}	*Clyne et al.* [1972]
$BrO + ClO \rightarrow Br + Cl$	7.04×10^{-12}	*Atkinson et al.* [2004]
$BrO + ClO \rightarrow BrCl$	1.15×10^{-12}	*Atkinson et al.* [2004]
$BrO + ClO \rightarrow Br + OClO$	9.06×10^{-12}	*Atkinson et al.* [2004]
$HOBr + OH \rightarrow BrO + H_2O$	5.0×10^{-13}	*Kukui et al.* [1996]
$HOBr + Cl \rightarrow BrCl + OH$	8.0×10^{-11}	*Kukui et al.* [1996]
$HOBr + O(^3P) \rightarrow BrO + OH$	2.12×10^{-11}	*Atkinson et al.* [2004]
$IO + BrO \rightarrow Br + OIO$	9.36×10^{-11}	*Atkinson et al.* [2004]
$IO + BrO \rightarrow IBr$	4.32×10^{-11}	*Atkinson et al.* [2004]
$IO + BrO \rightarrow Br + I$	7.2×10^{-12}	*Atkinson et al.* [2004]

Photolysis Reactions	J_{max} **(25 March)** s^{-1}	**Lifetime**	**Reference**
$BrNO_3 \rightarrow Br + NO_3$	2.1×10^{-4}	1.3 h	calculated from OASIS data
$BrNO_3 \rightarrow BrO + NO_2$	1.2×10^{-3}	14.2 min	calculated from OASIS data
$BrO \rightarrow Br + O(^3P)$	3.0×10^{-2}	33 s	calculated from OASIS data
$Br_2 \rightarrow Br + Br$	4.4×10^{-2}	23 s	calculated from OASIS data
$HOBr \rightarrow Br + OH$	2.3×10^{-3}	7.2 min	calculated from OASIS data
$BrNO_2 \rightarrow Br + NO_2$	1.5×10^{-4}	1.8 h	estimate from *Lehrer et al.* [2004]

$BrCl \rightarrow Br + Cl$	1.26×10^{-2}	1.3 min	calculated from OASIS data	

Mass Transfer Reactions	k_t **(forward)**	k_t **(reverse)**
$HBr_{(g)} \rightarrow H^+_{(p)} + Br^-_{(p)}$	1.80×10^{-3}	
$HCl_{(g)} \rightarrow H^+_{(p)} + Cl^-_{(p)}$	2.58×10^{-3}	
$HOBr_{(g)} \rightarrow HOBr_{(p)}$	1.26×10^{-3}	
$BrNO_{2(g)} \rightarrow BrNO_{2(p)}$	1.26×10^{-3}	
$BrONO_{3(g)} \rightarrow BrONO_{3(p)}$	1.26×10^{-3}	
$Br_{2(g)} \leftrightarrow Br_{2(p)}$	1.78×10^{-5}	2.97×10^{8}
$BrCl_{(g)} \leftrightarrow BrCl_{(p)}$	6.60×10^{-4}	1.91×10^{10}
$IBr_{(p)} \rightarrow IBr_{(g)}$	5.53×10^{9}	
$HBr_{(g)} \rightarrow H^+_{(s)} + Br^-_{(s)}$	1.67×10^{-5}	
$HCl_{(g)} \rightarrow H^+_{(s)} + Cl^-_{(s)}$	1.67×10^{-5}	
$HOBr_{(g)} \rightarrow HOBr_{(s)}$	1.67×10^{-5}	
$BrNO_{2(g)} \rightarrow BrNO_{2(s)}$	1.67×10^{-4}	
$BrONO_{3(g)} \rightarrow BrONO_{3(s)}$	1.26×10^{-4}	
$Br_{2(g)} \leftrightarrow Br_{2(s)}$	1.0×10^{-5}	7.71×10^{-2}
$BrCl_{(g)} \leftrightarrow BrCl_{(s)}$	1.25×10^{-5}	7.71×10^{-2}
$IBr_{(s)} \rightarrow IBr_{(g)}$	7.71×10^{-2}	

Aqueous Phase Reactions	k **(particle)**	k **(snow)**	**Reference**
$Cl^- + HOBr + H^+ \rightarrow BrCl$	5.17×10^{-21}	9.30×10^{-26}	*Wang et al.* [1994]
$Br^- + HOCl + H^+ \rightarrow BrCl$	1.2×10^{-24}	2.15×10^{-29}	*Sander et al.* [1997]
$Br^- + HOBr + H^+ \rightarrow Br_2$	1.47×10^{-20}	2.64×10^{-25}	*Beckwith et al.* [1996]
$Br^- + HOI + H^+ \rightarrow IBr$	3.04×10^{-18}	5.46×10^{-23}	*Troy et al.* [1991]
$BrCl + Cl^- \rightarrow BrCl_2^-$	3.3	5.99×10^{-5}	*Michalowski et al.* [2000]
$BrCl_2^- \rightarrow BrCl + Cl^-$	1.58×10^{9}	1.58×10^{9}	*Michalowski et al.* [2000]
$BrCl + Br^- \rightarrow Br_2Cl^-$	3.3	5.99×10^{-5}	*Michalowski et al.* [2000]
$Br_2Cl^- \rightarrow BrCl + Br^-$	3.34×10^{5}	3.34×10^{5}	*Wang et al.* [1994]
$Cl_2 + Br^- \rightarrow BrCl_2^-$	4.27	7.66×10^{-5}	*Wang et al.* [1994]
$BrCl_2^- \rightarrow Cl_2 + Br^-$	6.94×10^{2}	6.94×10^{2}	*Wang et al.* [1994]
$O_3 + Br^- \rightarrow HOBr$	4.5×10^{-9}	8.08×10^{-14}	*Oum et al.* [1998]

Table 2. Median mid-day bromine chain lengths for 25, 29, and 30 March 2009 (days with O_3 present) determined for four different modeling scenarios with different combinations of halogens present. Method 1 refers to Equation 3 (using terminations reactions) and Method 2 refers to Equation 4 (using initiation reactions).

	25 March		29 March		30 March		Average (1-σ st. deviation)	
	Method 1	Method 2	Method 1	Method 2	Method 1	Method 2	Method 1	Method 2
Br only	1.25	0.85	1.51	1.10	1.79	1.40	1.52 (± 0.27)	1.11 (± 0.28)
Br and Cl (Base)	1.29	0.84	1.43	1.03	1.58	1.29	1.43 (± 0.14)	1.05 (± 0.22)
Br and Low I	1.37	0.86	1.60	1.12	1.82	1.41	1.59 (± 0.22)	1.13 (± 0.28)
Br, Cl, and I	1.37	0.87	1.51	1.04	1.65	1.31	1.51 (± 0.14)	1.07 (± 0.23)

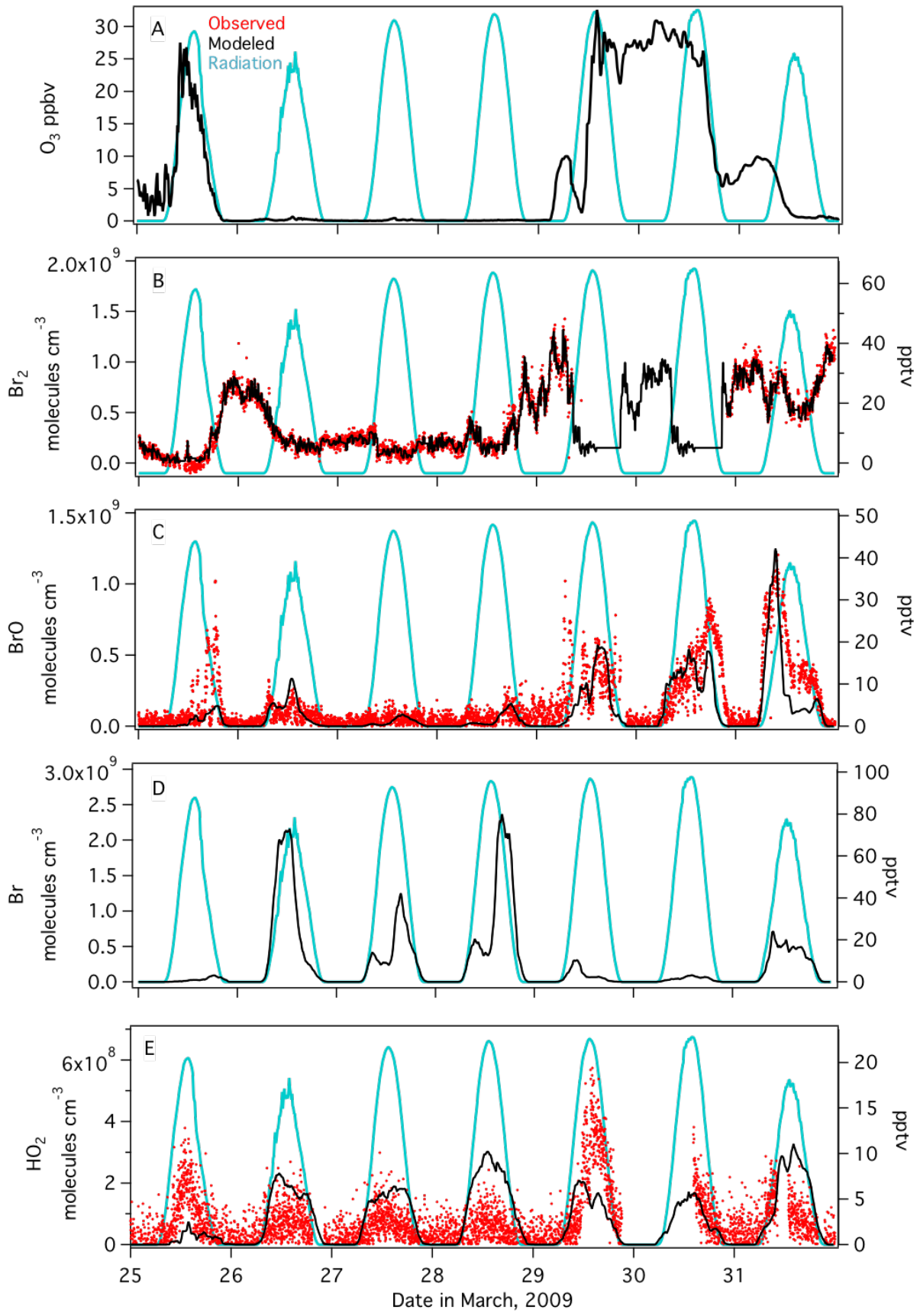
A
Observed
Modeled
Radiation
O_3 ppbv
B
Br_2 molecules cm^{-3}
ppt$v$
C
BrO molecules cm^{-3}
ppt$v$
D
Br molecules cm^{-3}
ppt$v$
E
HO_2 molecules cm^{-3}
ppt$v$
Date in March, 2009

1207

Fig 1. Time-series of gas-phase concentrations and mixing ratios of O_3, Br_2, BrO, Br, and HO_2 in the model (black trace) for the seven-day period simulated. Observations are plotted in red where available for Br_2, BrO, and HO_2. O_3 and Br_2 are constrained species in the model. Simulated output of BrO, Br, and HO_2 are smoothed by hourly averaging. Radiation is shown as the cyan trace as a reference. Time is expressed in Alaska Standard Time.

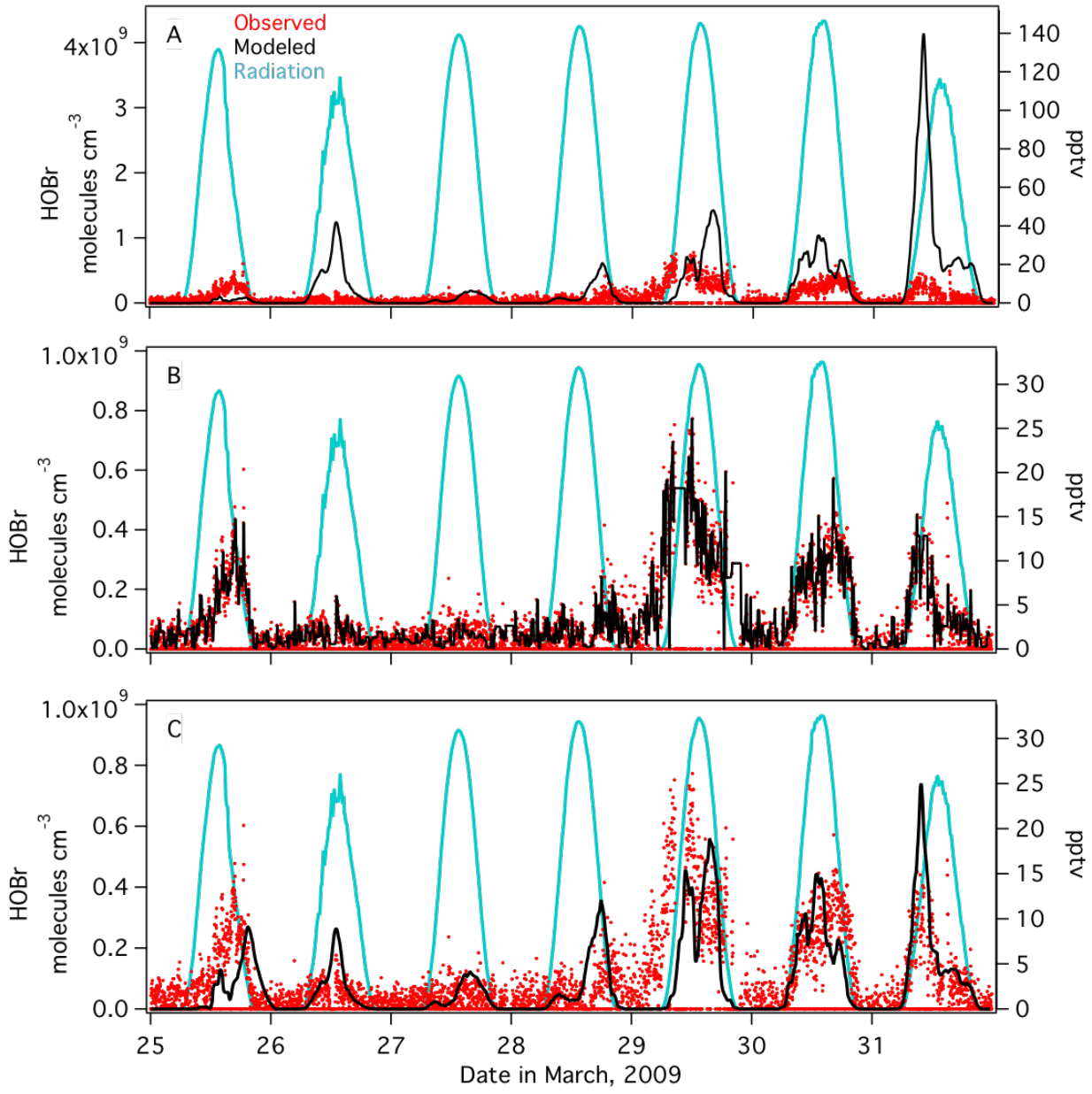

Fig 2. Simulated (black trace) versus observed (red markers) HOBr mixing ratios shown for three different versions of the model: A) HOBr unconstrained and allowed to freely evolve with a constant surface deposition term as described in the Methods, B) HOBr constrained to observations, C) HOBr unconstrained but with a variable surface deposition that is enhanced during higher wind speeds. Simulated (unconstrained) output in Panels A and C are smoothed by

hourly averaging. Radiation is shown as the cyan trace as a reference. Time is expressed in Alaska Standard Time.

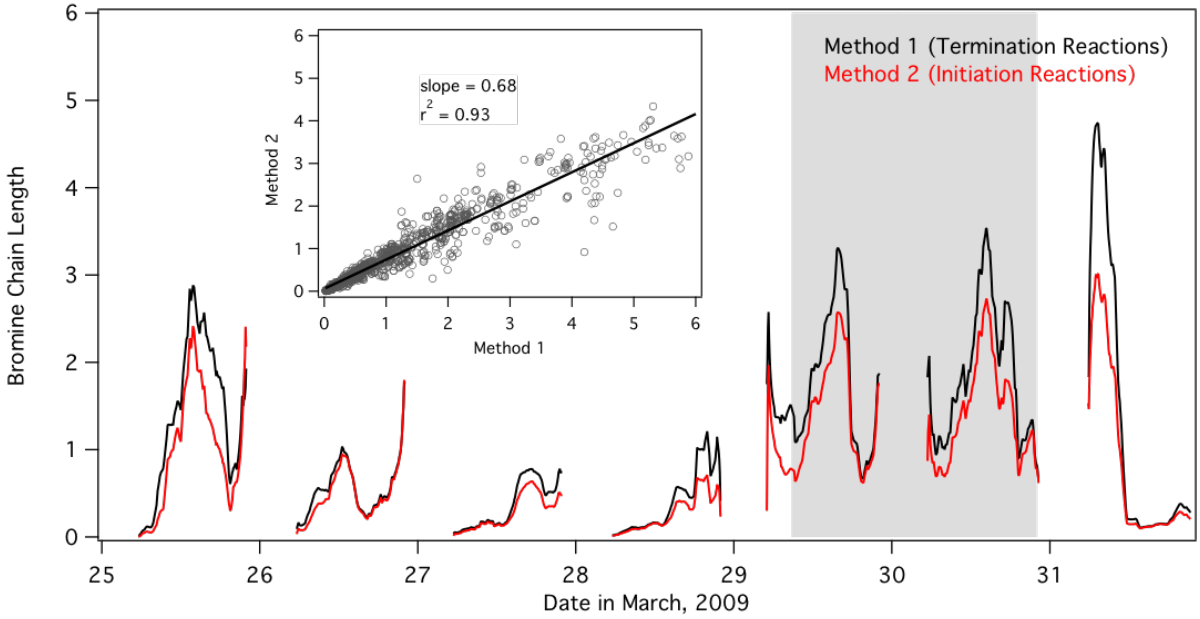

Fig 3. Time-series of model calculated bromine chain length for the daytime hours (7:00 to 21:00 AKST). Method 1 is plotted as the black trace and Method 2 is plotted as the red trace. Model output is smoothed by hourly averaging. The grey shaded box represents a period of missing Br_2 observations. The inset graph shows a linear regression of Method 1 and Method 2 calculations. Time is expressed in Alaska Standard Time.

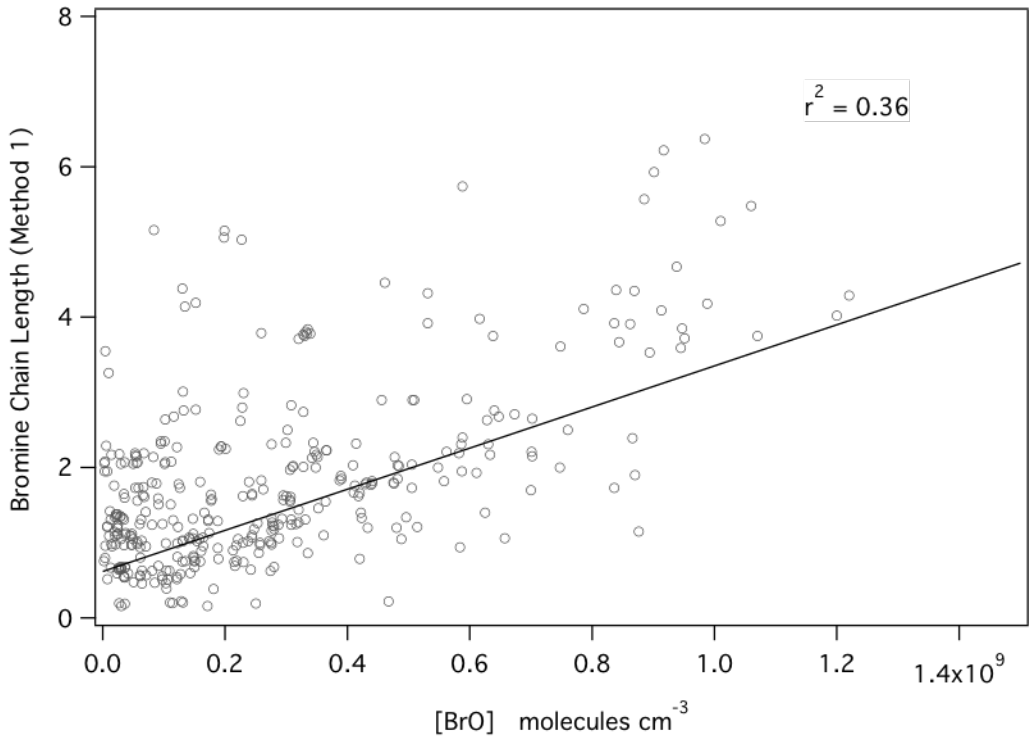

Fig 4. Regression of daytime (7:00 – 21:00 AKST) bromine chain length calculated by Method 1 (Equation 5) and simulated BrO concentration.

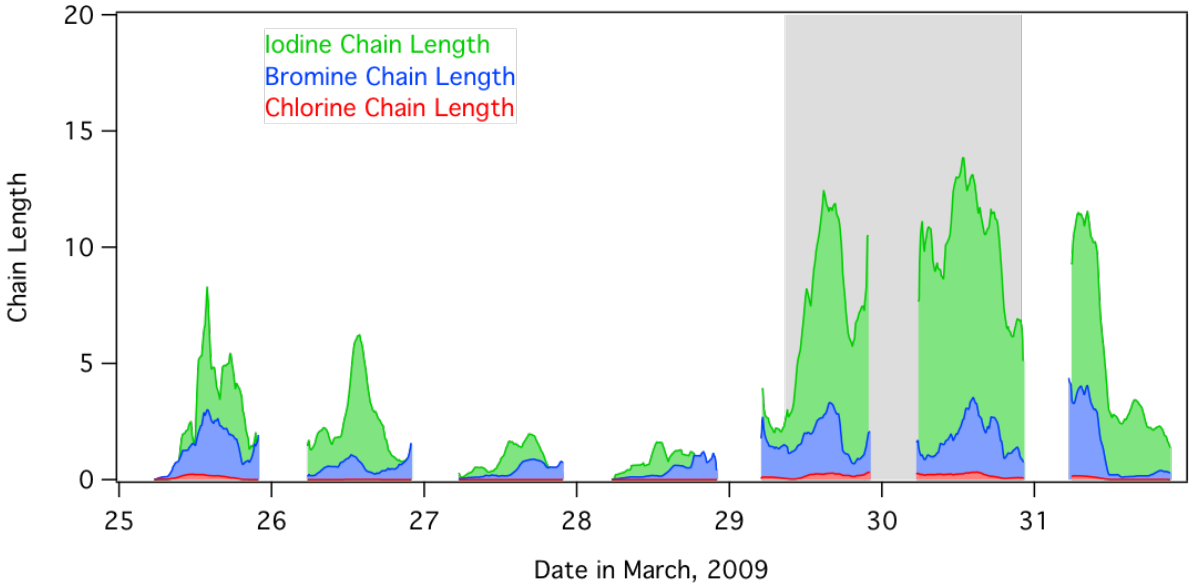

Fig 5. Calculated chain lengths for iodine (green), bromine (blue), and chlorine (red) across the seven days of the simulated period modeled using the Base + Iodine scenario. Model output is smoothed by hourly averaging. The grey shaded box represents a period of missing Br_2 observations. Time is expressed in Alaska Standard Time.

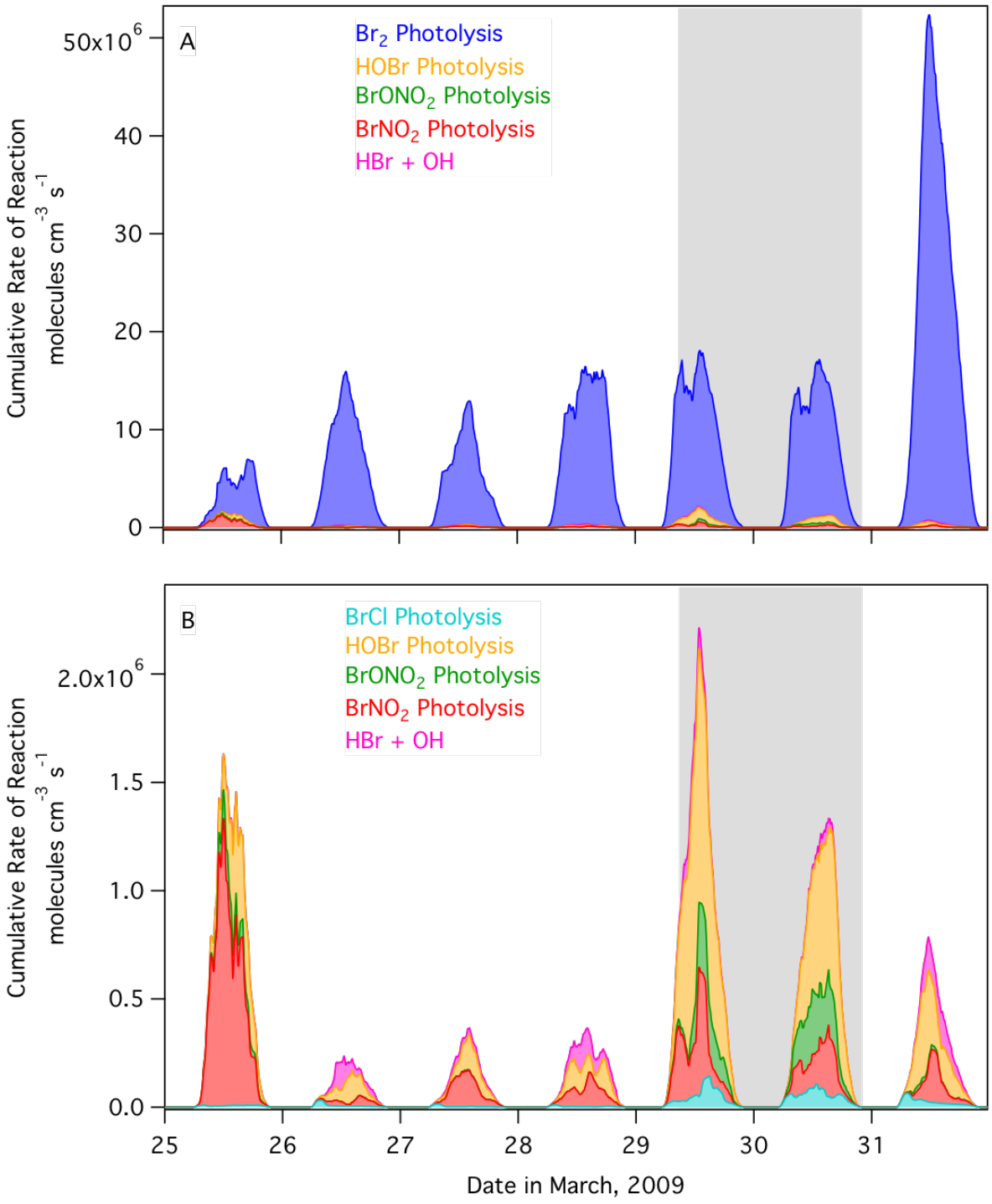

Fig 6. Time-varying rates of the most important bromine initiation reactions in the Base Model. Panel A includes photolysis of Br_2, which dominates the bromine initiation. Br_2 photolysis is calculated as 2 x $J_{Br2}[Br_2]$. In Panel B, Br_2 photolysis has been removed so that the minor terms can be visualized. Panel B also includes BrCl, which contributes only a negligible amount to

bromine initiation. Model output is smoothed by hourly averaging. The y-axis is expressed as a cumulative rate of reaction. The grey shaded box represents a period of missing Br_2 observations. Time is expressed in Alaska Standard Time.

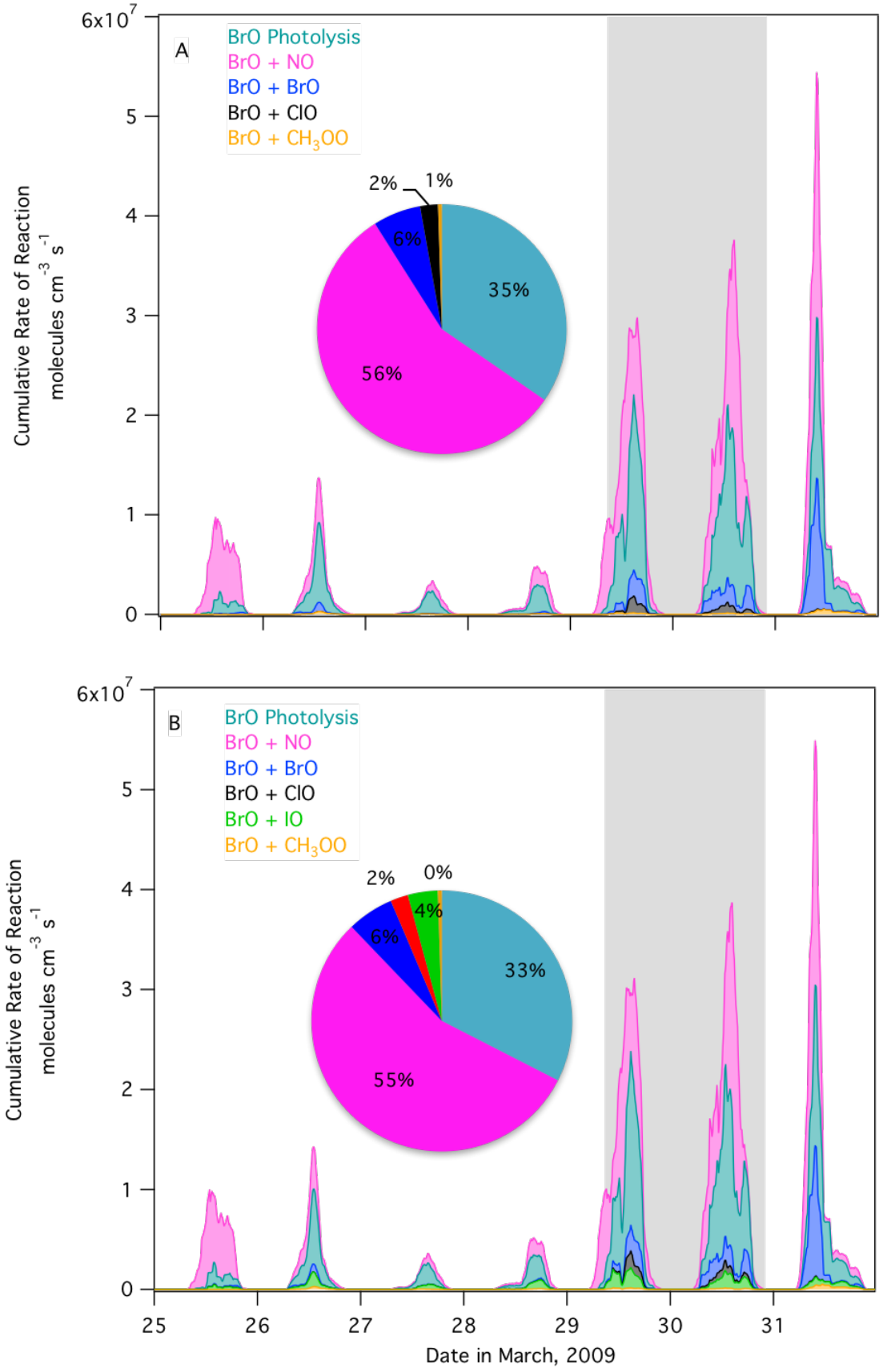
A
BrO Photolysis
BrO + NO
BrO + BrO
BrO + ClO
BrO + CH3OO
2%
1%
6%
35%
56%
6x10^7
5
4
3
2
1
0
Cumulative Rate of Reaction
molecules cm^-3 s^-1
B
BrO Photolysis
BrO + NO
BrO + BrO
BrO + ClO
BrO + IO
BrO + CH3OO
2%
0%
4%
6%
33%
55%
25
26
27
28
29
30
31
Date in March, 2009

1252

Fig 7. Time-varying rates of the most important bromine propagation reactions in the Base Model with Br and Cl present (Panel A) and with iodine included (Panel B). The BrO + BrO reaction is calculated as $2k[BrO]^2$ as this reaction regenerates two Br atoms. Model output is smoothed by hourly averaging. The y-axis is expressed as a cumulative rate of reaction. The grey shaded box represents a period of missing Br_2 observations. Time is expressed in Alaska Standard Time. The inset pie charts show the average fractional importance of each reaction pathway for only days 29 and 30 March (i.e. background O_3 days).

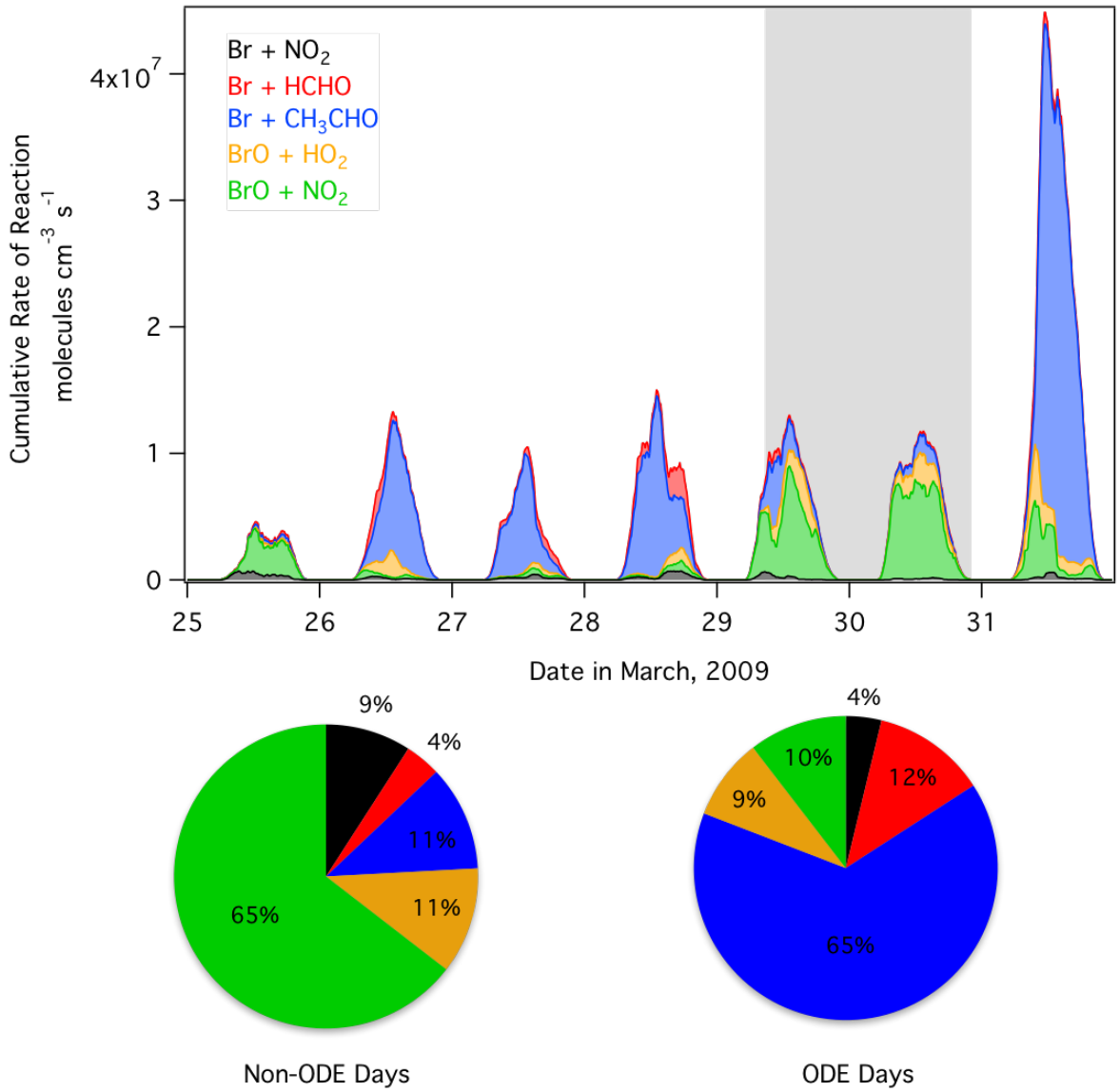

Fig 8. Time-varying rates of the most important reactive bromine (BrO_x) termination reactions in the Base Model. Model output is smoothed by hourly averaging. The y-axis is expressed as a cumulative rate of reaction. The grey shaded box represents a period of missing Br_2 observations. Time is expressed in Alaska Standard Time. The pie charts show the average fractional importance of each reactive bromine sink for non-ODE (background O_3) days and ODE days.

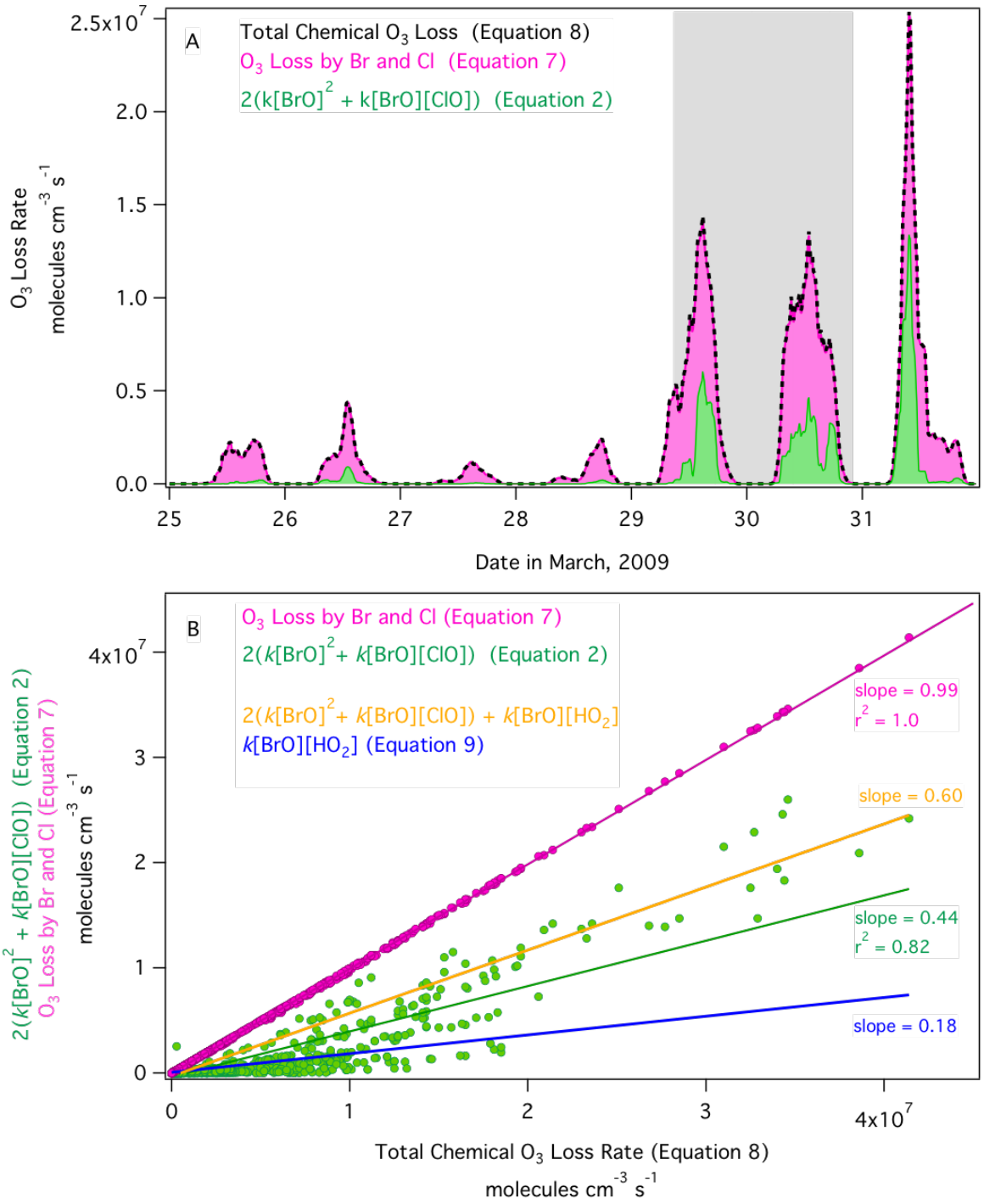

Fig 9. A) Comparison of the time-varying O_3 loss rate calculated using the estimation of $2(k[BrO]^2 + k[BrO][ClO])$ (Equation 2, green), the simulated O_3 loss rate by Br and Cl (Equation 7, pink), and the total simulated chemical O_3 loss rate (Equation 8, dashed black trace). Model output is smoothed by hourly averaging. The grey shaded box represents a period of missing Br_2 observations. Time is expressed in Alaska Standard Time. B) Shown is a regression of the

2(k[BrO]^2 + [BrO][ClO]) estimation method (Equation 2) versus the total simulated chemical O_3 loss rate in the Base Model (Equation 8) in the green data, and a regression of O_3 loss rate by Br and Cl only (Equation 7) versus the total simulated chemical O_3 loss rate in the pink data. The blue trace represents the O_3 loss rate estimated by only considering k[BrO][HO_2] (Equation 9). The orange trace estimates O_3 loss rate combining the three major gas-phase ozone depletion cycles. The slopes represent the fraction of the chemical O_3 loss rate that can be accounted for by each method. For the conditions simulated, the commonly used estimation method of 2(k[BrO]^2 + [BrO][ClO]) only accounts for 44% of the chemical O_3 loss rate.

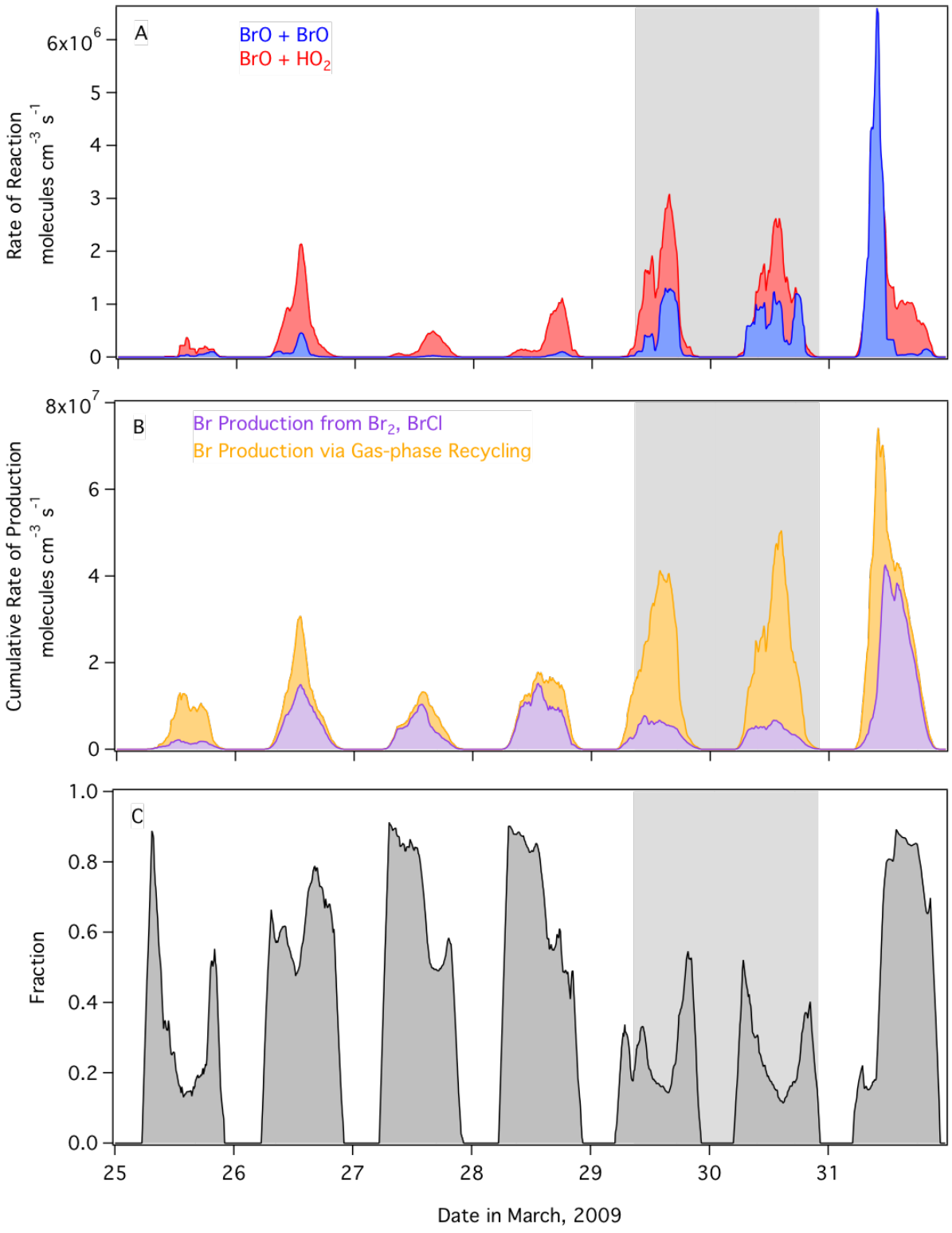

1283

1284 **Fig 10.** Panel A: Comparison of the rate of reaction of BrO + BrO (blue) and BrO + HO_2 (red).
1285 Panel B: The cumulative rate of Br atom production separated into the Br production rate from
1286 the photolysis of Br_2 and BrCl surface emissions calculated from Equation 10 (purple) and the Br

atom production rate due to gas-phase radical recycling calculated from Equation 11 (orange). Panel C: The fraction of total Br atom production due to production from Br_2 and BrCl surface emissions. In all panels, model output is smoothed by hourly averaging. The grey shaded box represents a period of missing Br_2 observations. Time is expressed in Alaska Standard Time.